

## General Disclaimer

### One or more of the Following Statements may affect this Document

- This document has been reproduced from the best copy furnished by the organizational source. It is being released in the interest of making available as much information as possible.
- This document may contain data, which exceeds the sheet parameters. It was furnished in this condition by the organizational source and is the best copy available.
- This document may contain tone-on-tone or color graphs, charts and/or pictures, which have been reproduced in black and white.
- This document is paginated as submitted by the original source.
- Portions of this document are not fully legible due to the historical nature of some of the material. However, it is the best reproduction available from the original submission.



**FLUIDICS**



CR 114333  
Available to the Public

**FLUIDIC PROPORTIONAL THRUSTER  
FOR  
SPARCS IV**

Contract NAS 2-5466

Prepared for:

National Aeronautics and Space Administration  
Ames Research Center  
Moffett Field, California

By:

T. S. Honda and W. L. Keltz  
General Electric Company  
Specialty Fluidics Operation  
Schenectady, New York



May 1971

**N71 - 32794**

FACILITY FORM 602

(ACCESSION NUMBER)

40

(THRU)

0-3

(PAGES)

CR-114333

(CODE)

31

(NASA CR OR TMX OR AD NUMBER)

(CATEGORY)

S-71-108

SPECIALTY FLUIDICS OPERATION  
**GENERAL ELECTRIC**

SCHENECTADY, NEW YORK

FLUIDIC PROPORTIONAL THRUSTER

FOR

SPARCS IV

Contract NAS 2-5466

Prepared for:

National Aeronautics and Space Administration  
Ames Research Center  
Moffett Field, California

By:

T.S. Honda and W.L. Keltz  
General Electric Company  
Specialty Fluidics Operation  
Schenectady, New York

May 1971

TABLE OF CONTENTS

	<u>Page</u>
List of Figures . . . . .	ii
List of Tables . . . . .	ii
Abstract . . . . .	iii
Introduction . . . . .	1
Synopsis . . . . .	4
Conclusion . . . . .	4
Recommendations . . . . .	4
Technical Discussion . . . . .	5
General . . . . .	5
Analysis . . . . .	5
Summary . . . . .	5
Discussion . . . . .	5
Hybrid Computer Simulation . . . . .	5
Noise Analysis . . . . .	13
Specification for Fluidic Proportional Thruster . . . . .	19
Hardware Implementation . . . . .	19
Summary . . . . .	19
Discussion . . . . .	19
Inspection Plan for Fluidic Proportional Thruster . . . . .	19
Thrust Nozzles . . . . .	20
Vortex Valve Specification . . . . .	20
Torque Motors . . . . .	21
Solenoid Valves . . . . .	23
Hardware Fabrication . . . . .	23
Summary . . . . .	23
Discussion . . . . .	23
Hardware Evaluation . . . . .	24
Summary . . . . .	24
Discussion . . . . .	24
Acceptance Test Procedure . . . . .	24
ATP Tests . . . . .	24



LIST OF FIGURES

<u>No.</u>		<u>Page</u>
1	FPT (Fluidic Proportional Thruster) . . . . .	3
2	SPARCS IV FPT (Circuit Diagram) . . . . .	7
3	SPARCS Mission Profile . . . . .	8
4	SPARCS Hybrid Computer Simulation . . . . .	10
5	FPT System Simulation (Pitch Axis) . . . . .	11
6	Tank Pressure vs Delivered Impulse . . . . .	11
7	Pitch Axis Thrust and Attitude During Planar Acquisition . . . . .	12
8	Simulated Thrust Blowdown for Typical Sun Acquisition . . . . .	12
9	Matrix of Acquisition Trials for SPARCS using FPT . . . . .	14
10	Matrix of Acquisition Trials for Standard SPARCS Control System . . . . .	14
11	Histogram of Gas Usage . . . . .	15
12	Histogram of Acquisition Time . . . . .	15
13	Pitch Control Loop . . . . .	16
14	SPARCS 150 FPT Vortex Valve Lamination . . . . .	22
15	SPARCS IV FPT (Outline) . . . . .	25
16	Plexiglas Model of FPT Manifold . . . . .	26
17	Functional Schematic of Laboratory Facility for Automating Phases I and II of ATP . . . . .	29
18	Functional Schematic of the FPT, Input Driving Signals and Output Transducers . . . . .	30
19	FPT ATP Test Set-up . . . . .	31
	FPT ATP Explosion Shield . . . . .	31
20	FPT ATP Connections for Charging the Blowdown Tank . . . . .	32
	FPT ATP Command Signal Generator . . . . .	32

LIST OF TABLES

1	FPT Mechanical, Pneumatic, Electrical and Performance Characteristics . . . . .	6
2	Model 121, D. G. O'Brien, Inc. SPARCS 150 Torque Motor Specifications . . . . .	21
3	FPT Functional Test Outline . . . . .	27

### ABSTRACT

This report summarizes the work performed for the National Aeronautics and Space Administration, Ames Research Center, Moffett Field, California, under Contract No. NAS 2-5466. The design, development, fabrication and acceptance test results of two fluidic proportional thrusters for use in the Solar Pointing Aerobee Rocket Control System are presented. A description of the three axis thruster control package utilizing vortex valves for proportional thrust modulation is also presented. The report contains a description of the acceptance procedure followed and the results of hardware evaluation.

## INTRODUCTION

This report summarizes the work performed under NASA Contract NAS 2-5466. The program included the design, development, fabrication and acceptance test evaluation of two flight worthy Fluidic Proportional Thrusters (FPT). The thrusters were designed in accordance with Specification A-15359 of April 1, 1969 and delivered for use in the Solar Pointing Aerobee Rocket Control System (SPARCS). The specified static and dynamic performance requirements were met with gas consumption well within the specified schedule. Performance results indicate capability of achieving 0.2 arcsecond peak to peak pointing stability or an order of magnitude improvement in current state-of-the-art pointing accuracy of sounding rocket payloads.

SPARCS is a sun-oriented attitude control system used in making scientific observations of the sun. It is a unique control system in that neither rate gyros nor an inertial platform are used for payload despin or sun acquisition. The result is a simple self-contained, light weight and accurate three-axis pointing system. SPARCS utilizes sun sensors as the primary source of pointing information. The attitude with respect to the third (roll) axis is measured with magnetometers. The outputs of the sensors are direction cosines to the payload-sun line and to the Earth's magnetic field vector, respectively. These signals are appropriately combined electronically to compute the attitude errors and vehicle rates and for formulation of the control law used as inputs for the pneumatic control system. The control torques are provided by cold-gas jets (Nitrogen, Freon, Argon, or Helium), which in SPARCS IV are modulated linearly by the Fluidic Proportional Thrusters during acquisition and for fine pointing.

SPARCS is a self-contained system and only the payload is controlled. It is designed to mate with the Aerobee or Black Brant launch vehicles. The payload which includes the SPARCS components and the rocket are separated a short time after burnout, after which the SPARCS control sequence is initiated to perform the two mission phases. The first, payload despin and solar acquisition, utilizes a direction cosine approach. The second, fine pointing, utilizes a fine sun sensor to achieve fine pointing. The resulting system is lighter in weight and more reliable than systems that use gyros and eliminates the careful handling, extensive component testing, and complex prelaunch updating required by gyros. With the exception of the pneumatic hardware, the system has no moving parts.

The Fluidic Proportional Thruster concept was conceived by NASA/ARC as a means of achieving an order of magnitude improvement in pointing accuracy of sounding rocket payloads. The initial investigation to demonstrate the feasibility of the concept was conducted previously under NASA Contract NAS 2-4490. The air bearing tests and analog simulation studies conducted indicated the feasibility of achieving pointing accuracy in the order of .1 arcsecond rms. The encouraging results led to the work reported herein.



The fluidic proportional thruster package developed in the program and shown in Figure 1 modulates control torques in three axes in response to electrical control signals from the SPARCS control electronic assembly (CEA) to orient the rocket payload to a command position. The FPT package also has the capability for adaptive control; i.e. selective switching between high and low thrust levels on command from the CEA.

The FPT package consists of three electromagnetic torque motors each operating a push-pull pair of vortex valves which provide thrust modulation about one of the three vehicle rotational axes. The package also contains four solenoid valves. One solenoid functions to activate supply gas flow from the tank to the FPT. Each axis has a solenoid valve to provide selective switching between high and low thrust levels. Three check valves are housed within the package to permit filling of the storage tank through one of the yaw channel outlets.

The specific program objective was to fabricate, test and deliver two FPT packages which are designed for flight missions in a SPARCS section. Orderly accomplishment of the program goals was achieved by effort in the following areas.

1. SPARCS - FPT performance, design and interface requirement definition.
2. Preparation and approval of the performance and design paragraphs of Specification A-15359.
3. Detail drafting of production drawings in accordance with Military Specification Mil-D-1000 Category E, Form 3.
4. Preparation and approval of acceptance test procedure.
5. Manufacture of two FPT packages including the conduct of quality assurance procedures in accordance with NASA Document NPC 200-3.
6. Acceptance testing of two FPT packages in conformance to the approved test procedure.

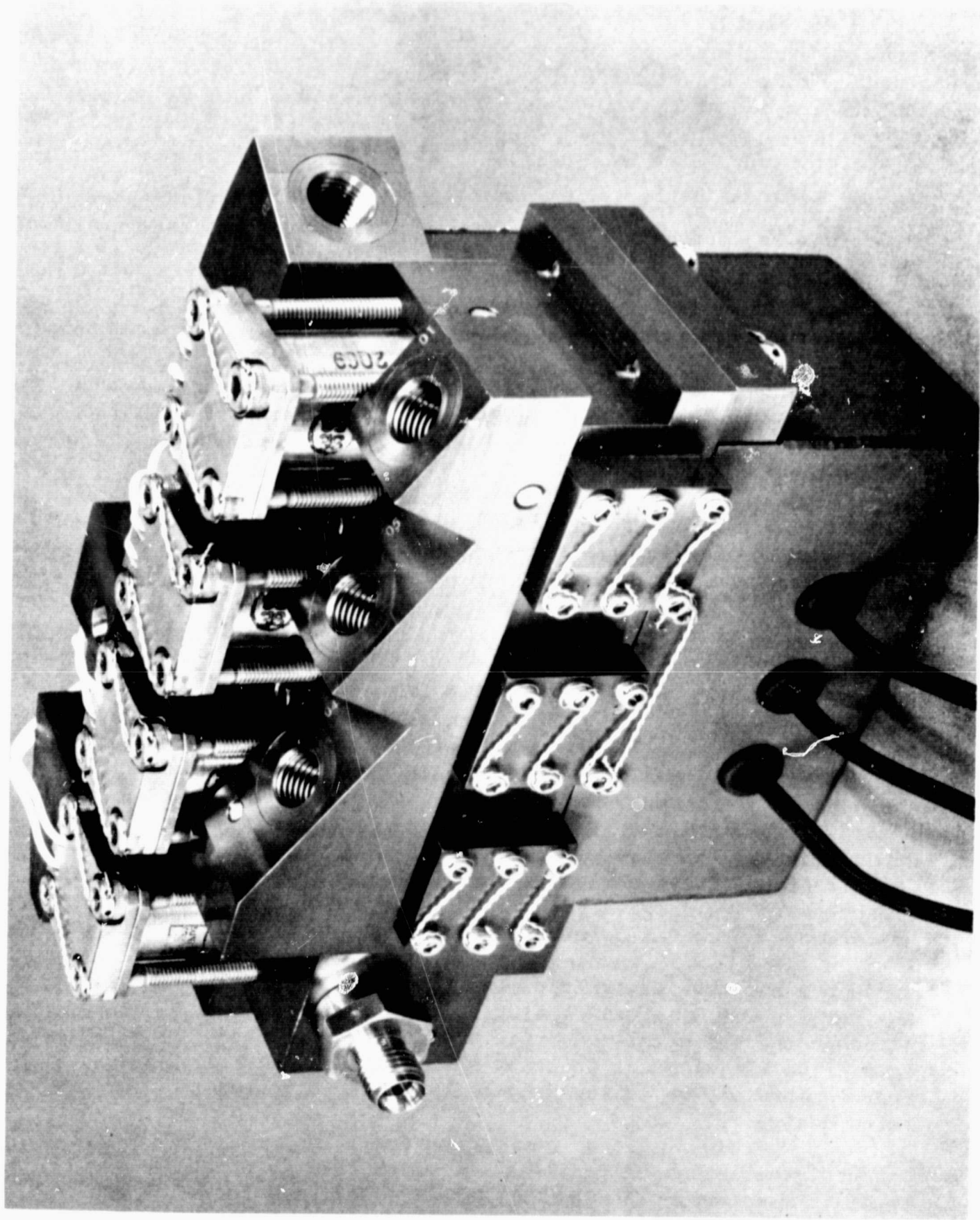


Figure 1 - Fluidic Proportional Thruster (FPT)



## SYNOPSIS

### CONCLUSION

The capability of the fluidic proportional thrusters (FPT) to position a SPARCS (Solar Pointing Aerobee Rocket Control System) payload so that the rms jitter is less than 0.2 arc second peak to peak was demonstrated. Such an angular jitter is equivalent to slightly more than the thickness of a quarter at a distance of one mile and improves by a factor greater than five the current best pointing stability for sounding rocket payloads. With this pointing stability the accuracy of scientific experiments conducted within sounding rocket payloads can be improved to the extent that they are competitive with those on more costly orbiting satellites.

The thruster static and dynamic performance requirements for successful acquisition on a typical SPARCS 150 mission are provided by the FPT with gas consumption well within the specified schedule. The specified tank volume of 200 cubic inches charged with 4500 - 5000 psig of Freon 14 was demonstrated to provide sufficient storage capacity to complete a nominal mission.

The FPT manufacturing techniques developed and utilized to fabricate two flight worthy FPT's proved the feasibility of future quantity production of FPT's with repeatable performance characteristics.

### RECOMMENDATIONS

The following recommendations for future work are submitted for consideration.

1. Demonstration of the FPT performance on Ames Research Center air bearing simulator.
2. Conduct SPARCS 150 mission flight tests utilizing the two fluidic proportional thrusters delivered on this program. Flight tests are necessary in order to evaluate system performance under real operating conditions.
3. Conduct a hardware design optimization study to minimize the noise power spectral density at the thruster output. Although the FPT developed on this program provides at least five times better pointing stability, further improvements may be achieved by refinements in vortex valve design.
4. Conduct studies for the application of the FPT to other specific missions. The SPARCS IV FPT is designed for a range of thrust requirements for that of SPARCS 150 up to that of SPARCS 350. The fluidic proportional thruster design can be adapted to larger thrust requirements with slight design modifications.

## TECHNICAL DISCUSSION

### GENERAL

The Fluidic Proportional Thruster (FPT) mechanical, pneumatic, electrical and performance characteristics are summarized in Table 1. The FPT is an electro-mechanical-fluidic device which furnishes three independent output thrusts which are proportional to the electrical input in contrast to a conventional thruster output whose thrust level is fixed. Providing a thrust proportional to an error signal is easily accomplished with the FPT by generating an electrical signal and applying it to the FPT input. Using a conventional thruster a proportional output can only be approximated by operating the thruster in an on-off mode and setting the on-time time to be proportional to the error signal. Pointing uncertainty in a Solar Pointing Aerobee Rocket Control System (SPARCS) with an FPT providing control thrusts is limited by thrust noise with a value of 0.2 arc second possible. A conventional on-off thruster in the same position loop leads to a pointing uncertainty which is in the form of a limit cycle. The limit cycle amplitude depends on the speed at which the thruster can be turned on and off with the amplitude decreasing as the speed increases. In the present SPARCS control a limit cycle amplitude of 1.0 arc second is possible. Therefore, the FPT improves by a factor of five the pointing uncertainty in a SPARCS control loop. The FPT electro-pneumatic circuit is shown schematically in Figure 2.

### ANALYSIS

#### Summary

A hybrid computer simulation of the FPT as part of the SPARCS verified its capability to successfully acquire the sun. An analysis of the effect of FPT thrust noise on attitude position uncertainty shows that an rms pointing uncertainty of 0.2 arc seconds is feasible. An FPT specification based on the requirements defined by the hybrid simulation and the noise analysis was submitted and approved.

#### Discussion

Hybrid Computer Simulation - The SPARCS mission profile is shown in Figure 3. The payload section is boosted to an altitude of approximately 200,000 ft where it separates from the rocket. Then the SPARCS positions the payload in pitch, yaw, and roll. The sun sensor establish the pitch and yaw reference and magnetometers establish the roll reference. A constant attitude is held for about 240 sec. The mission ends when aerodynamic forces overpower the available forces and tumbling occurs.

Table 1

FPT Mechanical, Pneumatic, Electrical and Performance Characteristics

Mechanical

Weight - 7 lbs

Space Envelope - 4 x 5 x 7½ in.

Mounting - five ¼ - 20 UNF tapped holes arranged for attachment to the skin of an Aerobee 15 in. diameter insert.

Pneumatic

Supply tank porting 7/16 - 20 UNF threaded hole

Three differential thrust output portings, five 7/16 - 20 UNF, and one 3/8 - 24 UNF threaded holes

Maximum tank pressure - 5000 psi

Operating medium - Freon 14, nitrogen, helium, or argon

Electrical

Four solenoids each requiring 1 amp at 28 volts

Three torque motors each with an input resistance of 125 ohms. The torque motor input shall not exceed 10.8 volts.

Performance

Maximum coarse roll thrust	4 lb	}	For a tank pressure of 5000 psi
Maximum fine roll thrust	0.2 lb		
Maximum coarse pitch (or yaw) thrust	2 lb		
Maximum fine pitch (or yaw) thrust	0.4 lb		
Fine roll gain	0.2 lb/volt	}	For a tank pressure of 2000 psi
Fine pitch (or yaw) gain	0.4 lb/volt		
Dynamic response - fine thrust level output lags a 2.0 Hz sinusoidal input by not more than 30 degrees.			



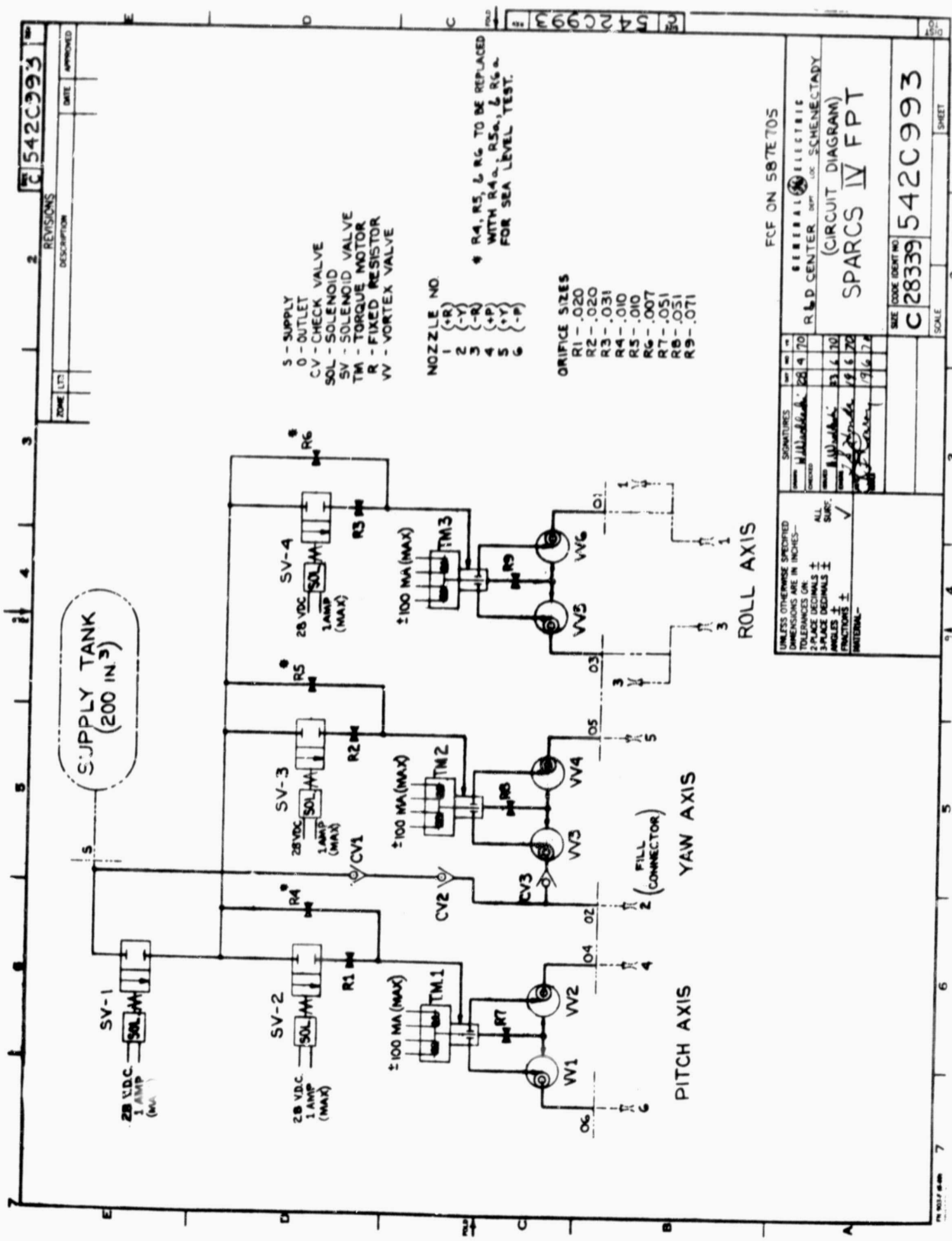


Figure 2 - SPARCS IV FPT (Circuit Diagram)

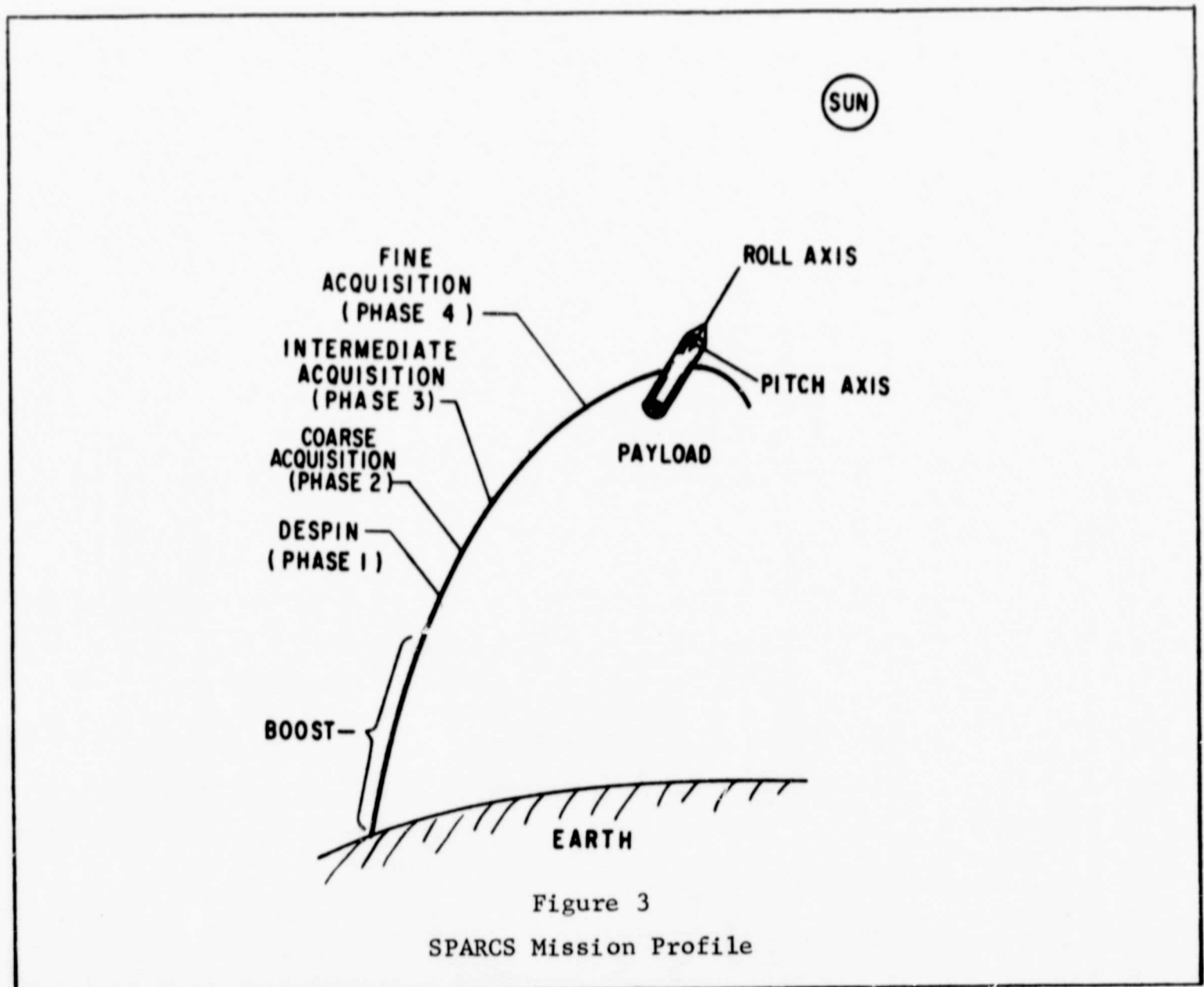


Figure 3  
SPARCS Mission Profile

The acquisition maneuver, shown in Figure 3, is separated into four phases as follows:

- Phase 1 - The payload is partially despun by a yo-yo from 2.5 to 1.0 rev/sec. Reaction control jets which are part of the FPT complete the despun to about 0 rev/sec.
- Phase 2 - Coarse acquisition is made in the pitch and yaw axis while the roll rate is held close to zero. Coarse acquisition ends when the pitch and yaw angles are both less than 10 degrees for one second.
- Phase 3 - Intermediate acquisition is used to position the vehicle in roll and complete sun acquisition to within 1 degree in pitch and yaw.
- Phase 4 - Fine acquisition is used to reduce the pitch and yaw errors to essentially zero and achieve fine pointing stability from an initial angle of about 1 degree.



A hybrid computer system is used to simulate 3-axis rotational motion of the SPARCS payload about a fixed center of gravity. Figure 4 is a block diagram of the simulation. Equations of motion for the payload and appropriate coordinate transformations are simulated with the analog computer. Attitude sensor signals obtained from the analog computer are sent to the SPARCS electronic breadboard. Error signals from the electronic breadboard for the roll, pitch, and yaw axes reenter the analog computer through the thruster portion of the simulation. The digital computer is used to set payload parameters and initial conditions for the analog computer. System performance data are monitored by the digital computer and statistically reduced.

Since gas consumption is a critical consideration associated with use of the proportional thruster, the thruster simulation was designed to include effects of tank pressure decay during sun acquisition. Figure 5 is a block diagram of the analog simulation representing the pitch axis of the fluidic proportional thruster system. In Figure 4, the conditions for  $|\delta y| > 1$  volt is equivalent to the pitch axis operation at high thrust level. Hence, the condition  $\delta p_1$  closed and  $\delta p_2$  open results in a rapid tank pressure decay time constant and simultaneously the conditions  $\delta p_3$  closed and  $\delta p_4$  open yields a high level pitch thrust. The conditions for  $|\delta y| < 1$  volt is conversely equivalent to operation at low thrust level and longer tank pressure decay time constant. The supply of Freon 14 in the tank is simulated so the maximum delivered impulse follows the analytically predicted value given in Figure 6.

The tank decay time constant depends on the amount of gas flowing from the control system nozzles. A simple adaptive thrust switching mechanism which measures the error signal magnitude of each axis to determine whether each respective axis is in the high or low thrust mode is used to conserve gas outflow.

If the magnitude of an input signal to an FPT channel exceeds one volt, then that channel is put into the coarse (or high level) thrust mode by actuating that channel's solenoid. For smaller input magnitudes the FPT remains in the fine thrust mode which reduces gas flow. This adaptive feature is instrumental in reducing gas flows during the despin, coarse and intermediate acquisition phases. Since the FPT input magnitude is used to switch back and forth from coarse to fine flow levels, this input is appropriately used to adjust the tank decay time constant. The signal representing tank pressure is used as a scale factor for determining available thrust in each axis.

Figure 7 shows pitch axis thrust and corresponding sine of the pitch attitude during a simulated pitch axis sun acquisition; high and low thrust modes demonstrating operation of the adaptive features are noted. Figure 8 shows available high thrust decaying during a typical simulated sun acquisition.

Because the equations of motion have time varying coefficients, acquisition performance of the system must be tested for a large number of different system initial conditions. Initial spin rates, payload inertias, and moment arms are

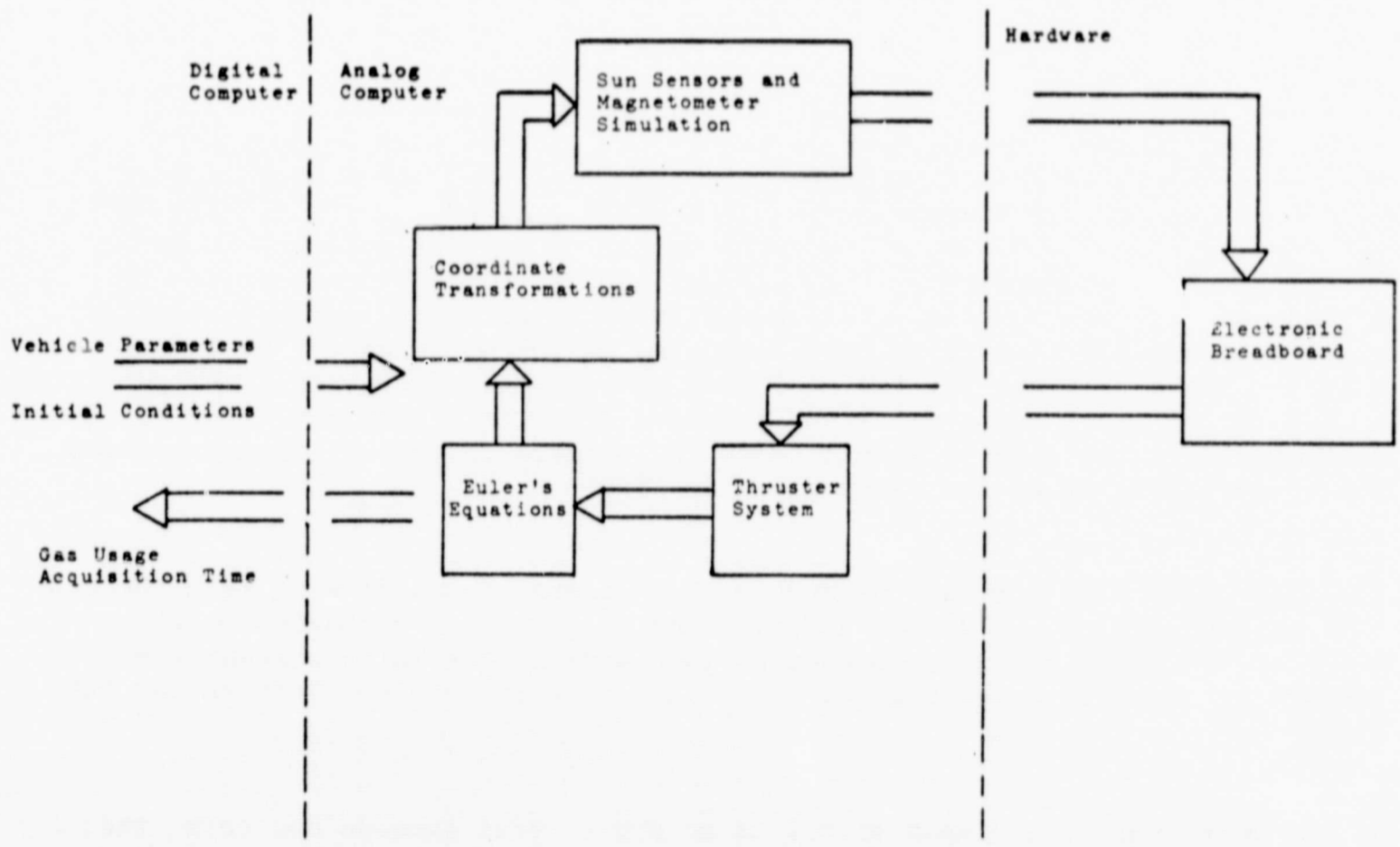


Figure 4 - SPARCS Hybrid Computer Simulation

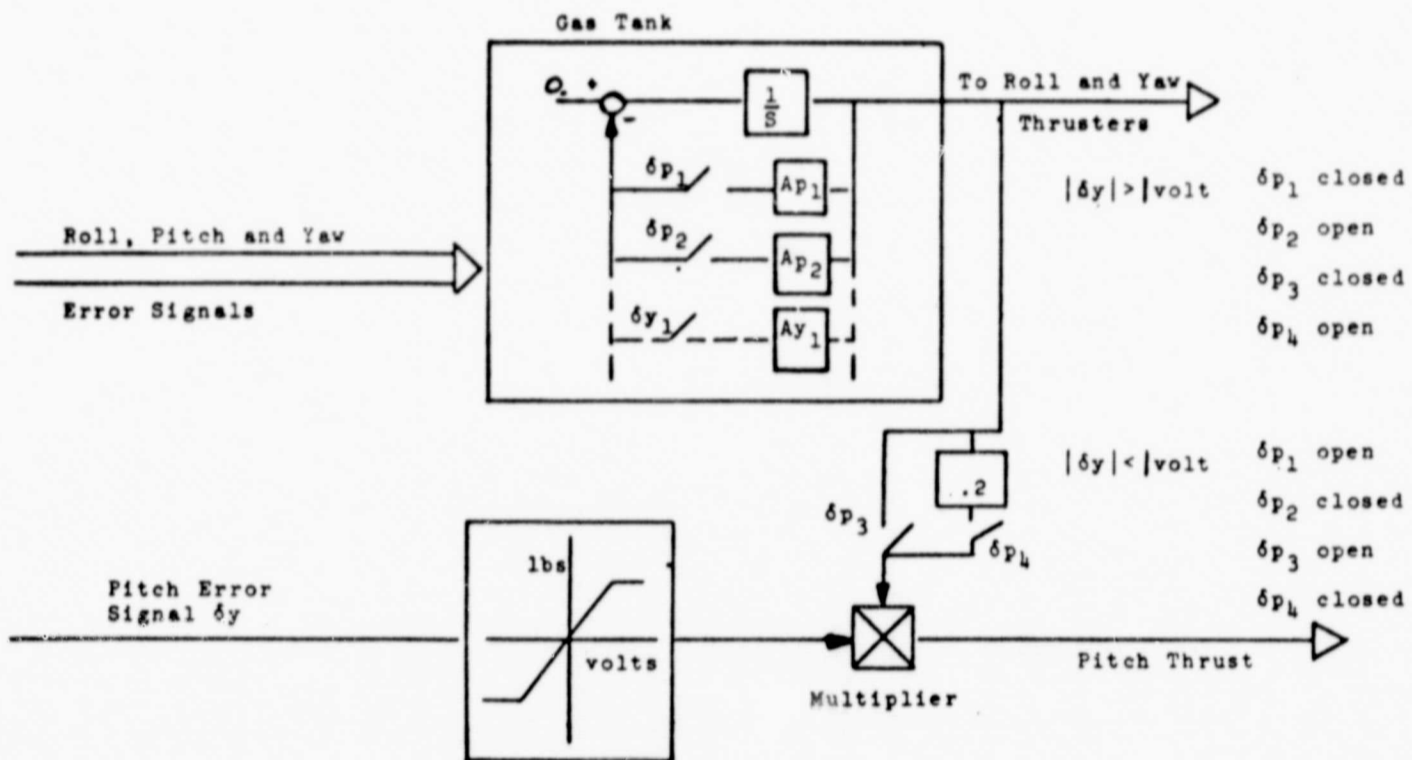


Figure 5 - FPT System Simulation (Pitch Axis)

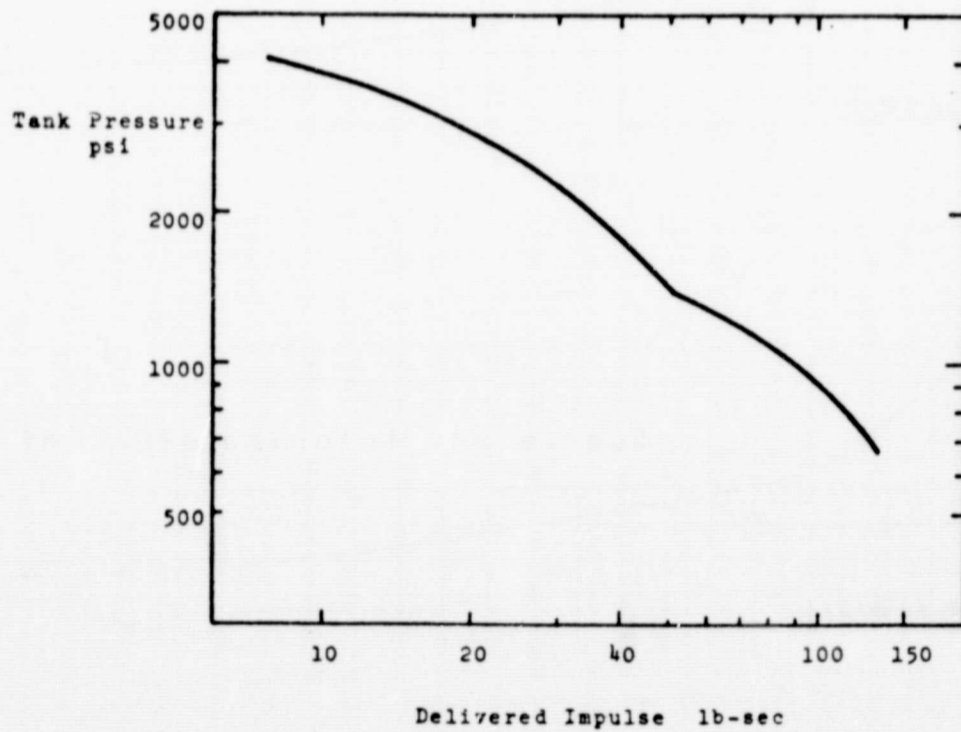


Figure 6 - Tank Pressure vs Delivered Impulse



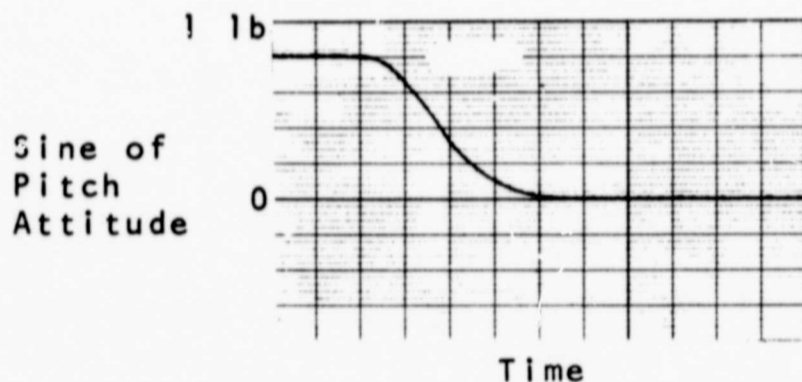
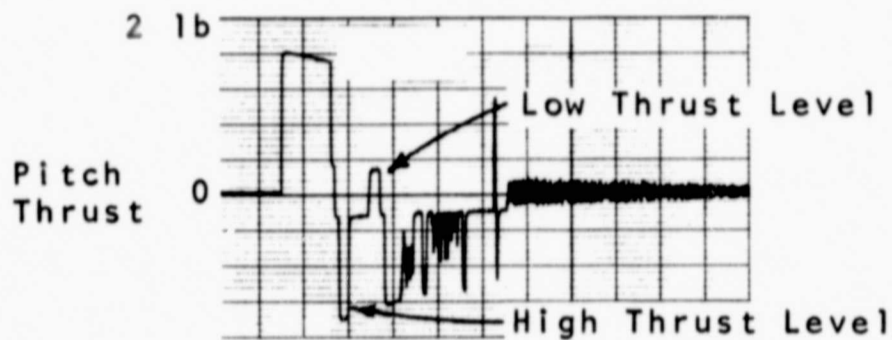


Figure 7 - Pitch Axis Thrust and Attitude During Planar Acquisition

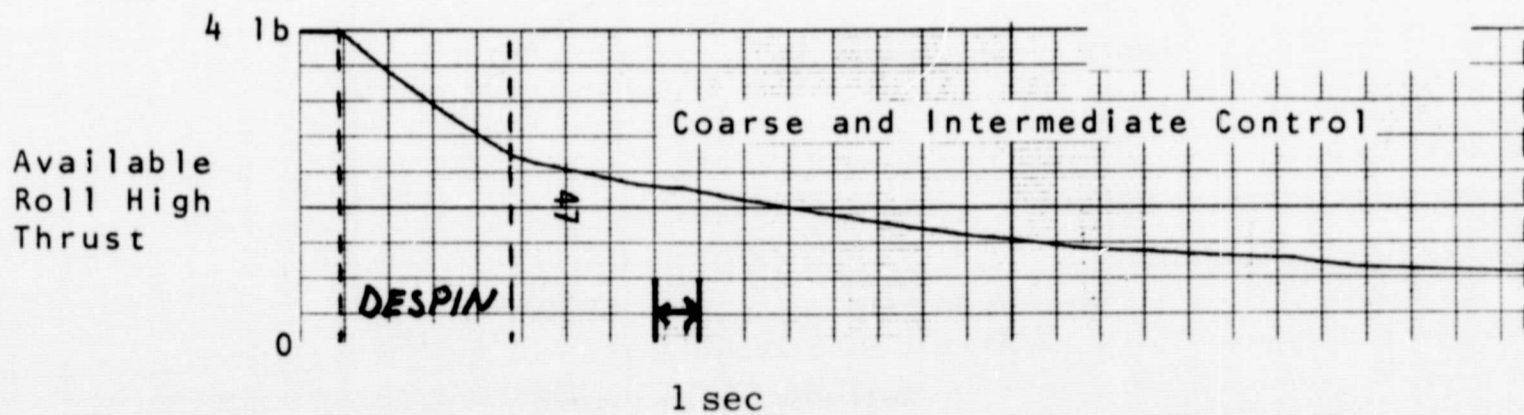
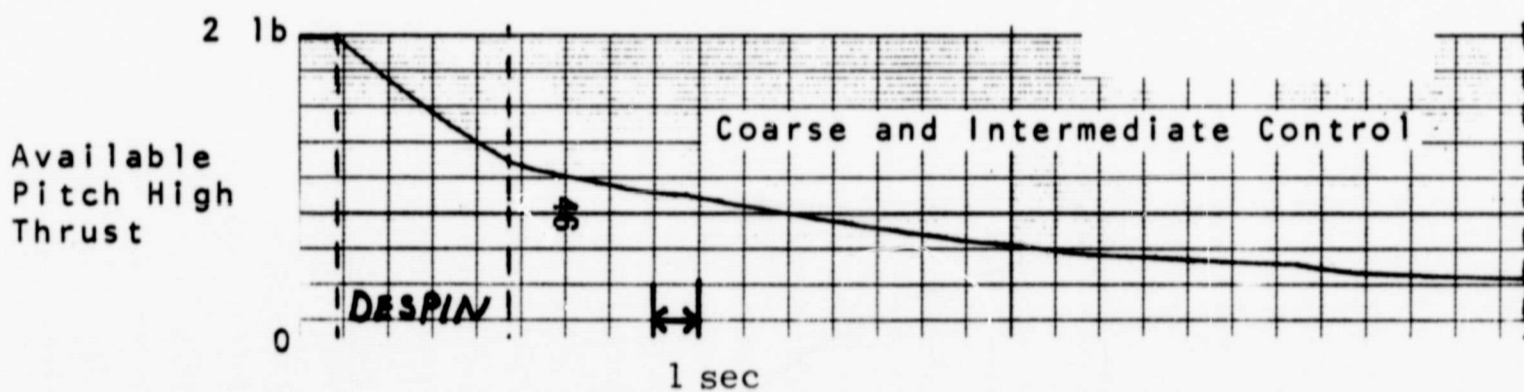


Figure 8 - Simulated Thrust Blowdown for Typical Sun Acquisition

typically held fixed during the acquisition tests. Eta angle ( $\eta$ ; angle between magnetic and sun vectors) and theta angle ( $\theta$ ; angle between payload momentum vector and sun vector) are the important initial conditions. Figures 9 and 10 are matrices of analog computer sun acquisitions for SPARCS with the FPT and the standard SPARCS attitude control system respectively; each square represents a different combination of  $\eta - \theta$ . Each square contains two numbers; one representing acquisition trials, the other acquisition successes. If the momentum vector of the payload is not aligned with the roll axis, the nose of the payload will trace out of a cone with the momentum vector as its center. The 21 acquisitions for each  $\eta - \theta$  pair represent control system initialization at 21 different locations around the cone. The portions of the  $\eta - \theta$  matrix filled in represent the most probable  $\eta - \theta$  pairs occurring at White Sands Missile Range, the normal SPARCS launch site.

Figures 11 and 12 present histograms of gas and time required for the acquisition trials shown in Figures 9 and 10. Comparison of the acquisition data shows that the FPT/SPARCS uses less gas during acquisition but takes somewhat longer to acquire the sun. Both systems display nearly the same success--attempt ratio. Both the standard SPARCS system and the FPT/SPARCS show acquisition failures when  $\eta$  approaches 180 deg. The roll axis rate signal is derived from a combination of magnetometer and sun sensor signals. When  $\eta$  is 180 deg, the sun and magnetic vectors are colinear and the roll axis rate computation is degraded resulting in a loss of roll axis control during sun acquisition. SPARCS is typically constrained from launching when  $\eta > 165$  deg.

The adaptive thrust switching mechanism is the primary reason for the gas usage reduction achieved by the FPT system. The FPT system uses lower thrust levels than the standard SPARCS; however, because the FPT utilizes continuous gas flow and the standard SPARCS uses on-off thrusters, no gas savings results from the lower thrust levels alone. Successful acquisition performance of the FPT system with the adaptive feature is comparable to the performance of the standard SPARCS system but at a reduction in gas usage. Examination of Figure 11 reveals that the adaptive mechanism saves approximately 20 lb-sec of gas during a typical sun acquisition. Figure 12 shows the FPT system requires about 6 sec more to acquire. This additional time is tolerable.

The salient fact which can be deduced from Figures 11 and 12 is that the continuous flow FPT with the adaptive control feature can replace the currently used on-off poppet valves. There is no need to install a larger Freon 14 supply tank and the predicted number of successful sun acquisitions is about the same for both systems.

Noise Analysis - The elements of the pitch control loop are shown in Figure 13. The yaw control is identical to the pitch control. The forward portion of the control loop consists of compensation, the FPT, the vehicle and two integrations. The feedback is provided by a sun sensor. During coarse control, switches S1 and S2 are closed while S3 and S4 remain open. The reverse occurs during intermediate and fine control.



$\theta \backslash n$	90°	45°	30°	10°	0°
90°	20 21	21 21	Successes Trials		
135°	21 21	21 21			
150°	21 21	21 21	21 21	21 21	22 22
160°			21 21	21 21	21 21
170°			20 21	22 22	
175°			14 21	16 21	

Figure 9 - Matrix of Acquisition Trials for SPARCS using FPT

$\theta \backslash n$	90°	45°	30°	10°	0°
90°	21 21	21 21	Successes Trials		
135°	21 21	21 21			
150°	21 21	21 21	21 21	21 21	21 21
160°			21 21	22 22	21 21
170°			19 21	21 22	
175°			17 21	16 21	

Figure 10 - Matrix of Acquisition Trials for Standard SPARCS Control System

Number of Successful  
Trial Acquisitions

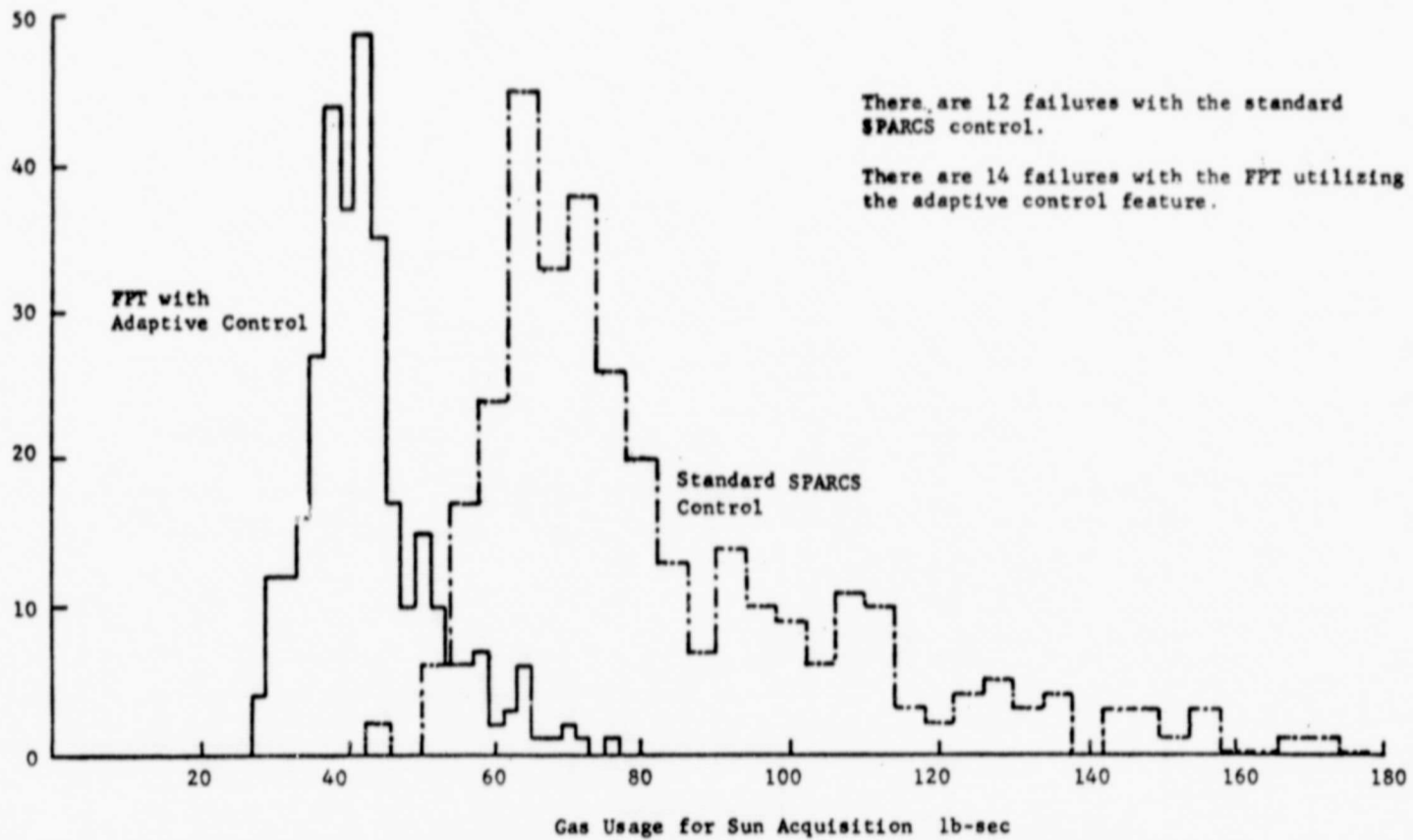


Figure 11 - Histogram of Gas Usage

Number of Successful  
Acquisition Trials

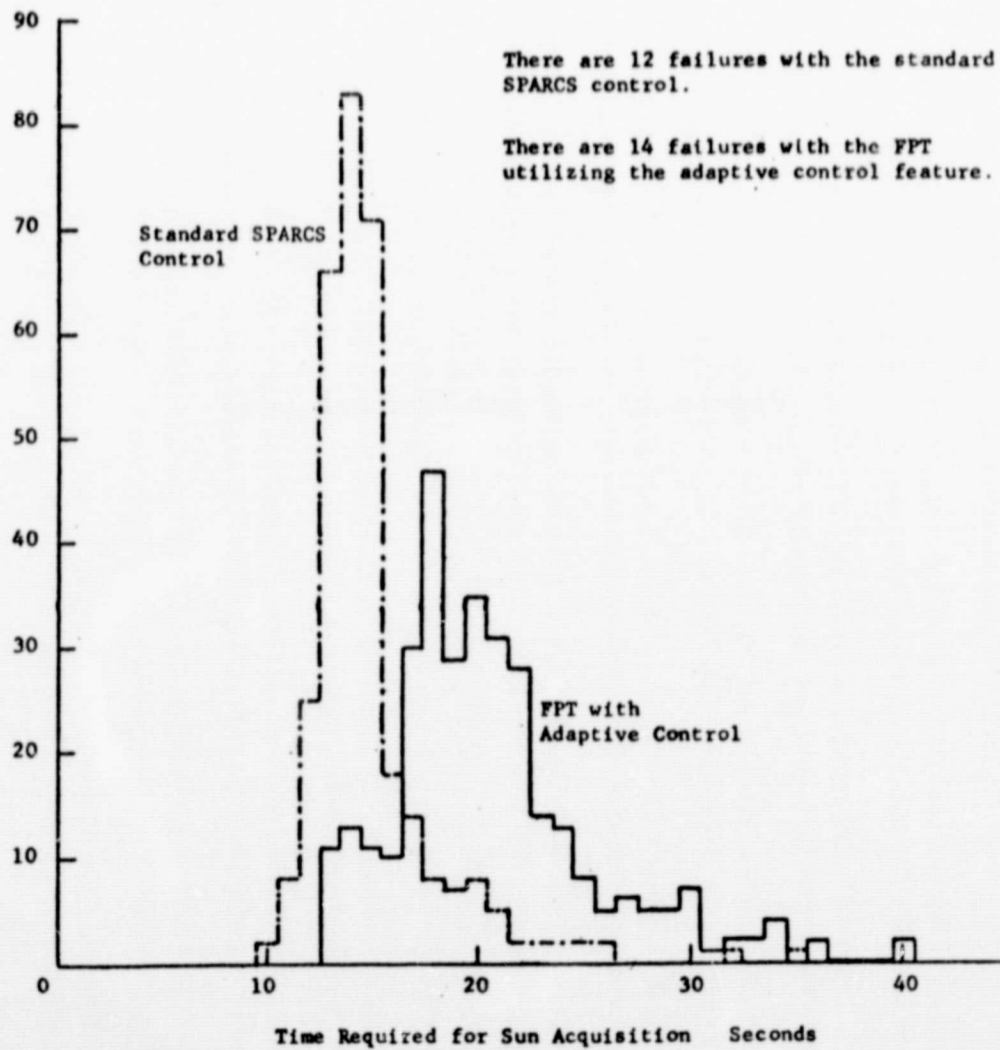


Figure 12 - Histogram of Acquisition Time

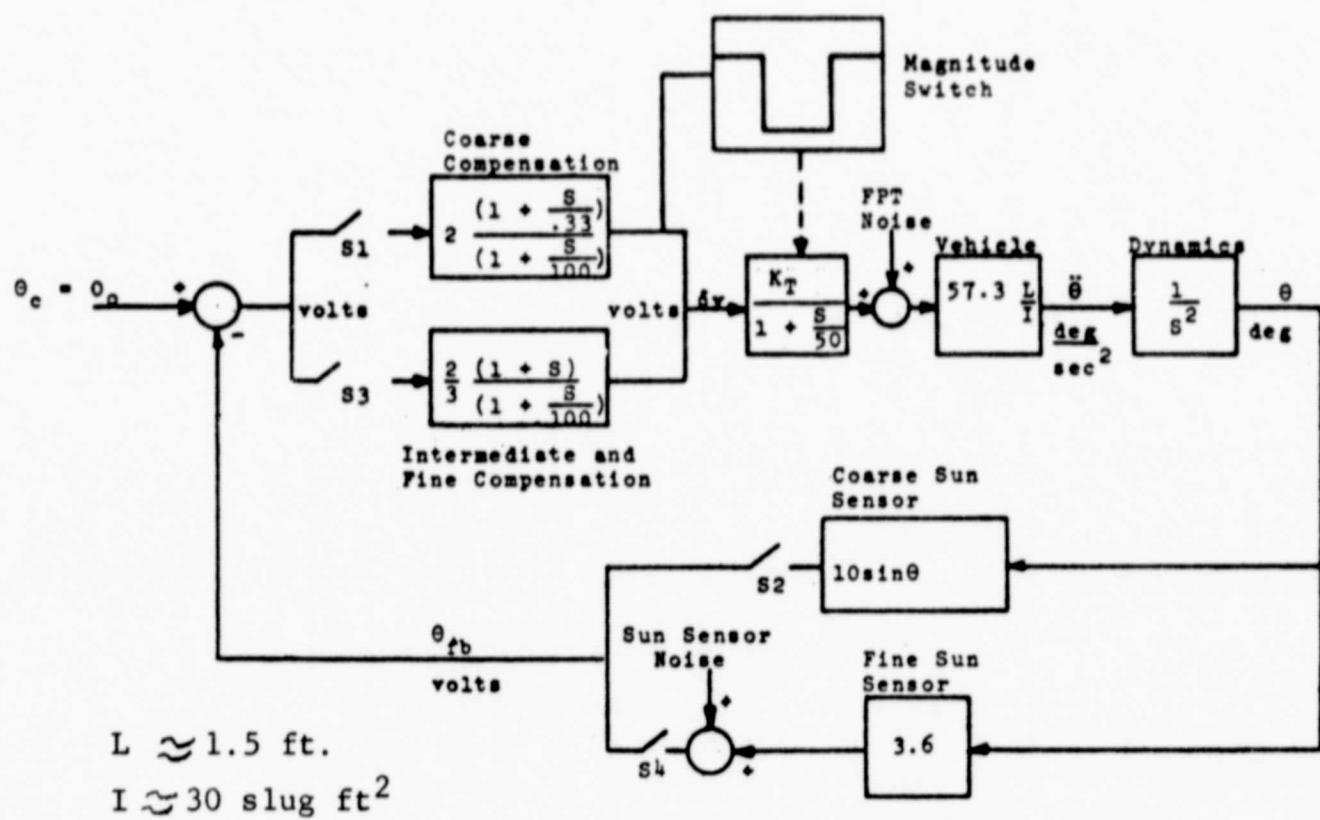


Figure 13 - Pitch Control Loop



The compensations are implemented electronically using integrated circuit operational amplifiers. The lead term in the compensation is necessary to stabilize the position loop. Analytically, the lead break frequency is roughly equivalent to the ratio of position to rate feedback. From Figure 13 one observes that the ratio of position to rate feedback during coarse control is 0.33 (volt/deg)/(volt per deg/sec) or simply 0.33 rad/sec. During intermediate and fine control the position to rate feedback is increased to 1 rad/sec. This makes the control loop more responsive to position commands, but more susceptible to fluidic thruster noise.

The output of the compensation drives the FPT torque motor and the coarse/fine thrust (magnitude) switch. The magnitude switch provides zero output if the magnitude of the compensation-output,  $|\delta y|$ , is less than 1 v. For zero pitch rate the magnitude switch output is zero if the error magnitude is less than about 3.4 degrees in coarse control or 0.4 degrees in intermediate and fine control. If  $|\delta y| > 1$  v, then the magnitude switch output is 28 v. The magnitude switch output drives a solenoid valve in the FPT which is energized by the 28 v signal. This energization causes a larger gas flow through the FPT thereby producing more thrust. It also increases the FPT gain,  $K_T$ , enough to make the FPT output normally at a plus or minus saturation level. For the pitch and yaw channels this level is about 1 lb at 1500 psig tank pressure. This thrust level is required when the error is large and results in rapid depletion of gas in the supply tank. By switching to the lower fine thrust level for  $|\delta y| < 1$  volt the control manages to reduce the gas flow and conserve fuel. Hybrid computer simulations validated the ability of the position loop with the magnitude switch to both control the vehicle position and significantly reduce Freon 14 fuel consumption.

The vehicle moment arm and moment of inertia (approximately 1.5 ft and 30 slug ft<sup>2</sup> respectively) are values which are not easily changed. These values correspond to an Aerobee 150 payload.

Two sun sensors (coarse and fine) are used because a single sensor cannot cover the large range from 90 deg to less than 0.1 arc second. The coarse sun sensor is used until both pitch and yaw errors are less than 10 deg at which time the sensing is switched to the fine sun sensor.

Figure 13 shows two noise sources. One is at the FPT output which is the noise inherent in the thruster and tends to increase as the saturation thrust level is increased. Thus, reducing the maximum available thrust decreases noise from this source. This approach corresponds to the solution for reducing a limit cycle amplitude by decreasing the amplitude of a bang-bang thruster. The second noise source is at the output of the fine sun sensor. The sources of the power spectral density content of the fine sun sensor are the sun itself and the electronics which make up the sensor. The relative contributions to the sensor spectral density have not been measured, but the noise generated by the sun imposes a lower limit on the ultimate accuracy of any solar pointing position loop. There is noise produced elsewhere in the control loop, but these sources have been omitted because they either apply to coarse control only or they can be referred to one of the two noise sources shown.

The effect the noise sources have on the uncertainty of the pitch position is given approximately by the following equations which are derived by using conventional analytic techniques.

$$\Theta_{T_{rms}} = \frac{1}{(KH)} \left( 57.3 \frac{L}{I} \right) \sqrt{\frac{\pi \omega_1 P_T(\omega)}{2}} \quad (1)$$

$$\Theta_{S_{rms}} = \frac{1}{H} \sqrt{\frac{\pi}{2 \omega_1} (KH + \omega_1^2) P_S(\omega)} \quad (2)$$

$\Theta_{T_{rms}}$  and  $\Theta_{S_{rms}}$  are the rms pointing uncertainties due to the thruster and sensor noise sources respectively.  $K$  is the forward loop gain with the  $1/S^2$  term omitted and  $H$  is the feedback gain.  $KH$  then is the loop gain at a frequency of 1 rad/sec.  $P_T(\omega)$  and  $P_S(\omega)$  are the noise power spectral densities of the FPT and fine sun sensor outputs respectively.  $\omega_1$  is the compensation lead break frequency.

From Equations (1) and (2) one concludes that increasing the feedback gain,  $H$ , (that is, the fine sun sensor gain) decreases both  $\Theta_{T_{rms}}$  and  $\Theta_{S_{rms}}$  thereby improving the pointing accuracy. Increasing  $KH$  by increasing  $K$  only reduces  $\Theta_{T_{rms}}$  directly but increases  $\Theta_{S_{rms}}$  by the square root of the increase. Increasing  $\omega_1$  increases  $\Theta_{T_{rms}}$  and  $\Theta_{S_{rms}}$  if  $\omega_1^2 > KH$ . Using values from Figure 13:

$$KH = \frac{2}{3} \times 1.3 \times \frac{57.3}{30} \times 1.5 \times 3.6 = 9.0 \frac{1}{\text{sec}^2}$$

$$H = 3.6 \text{ V/deg}$$

$$\omega_1 = 1 \text{ rad/sec}$$

$$P_T(\omega) = 1.5 \times 10^{-8} \frac{\text{lb}^2}{\text{rad/sec}} \text{ representative value}$$

$$P_S(\omega) \approx \frac{(10^{-4} \text{ V})^2}{500 \text{ rad/sec}} = 2 \times 10^{-11} \frac{\text{V}^2}{\text{rad/sec}}$$

representative value

$$L = 1.5 \text{ ft}$$

$$I = 30 \text{ slug ft}^2 = 30 \text{ ft lb sec}^2$$



Then:

$$\begin{aligned}\Theta_{T_{rms}} &= \frac{1}{9.0} \times \left(57.3 \times \frac{1.5}{30}\right) \sqrt{\frac{\pi \times 1 \times 1.5 \times 10^{-8}}{2}} \\ &= .489 \times 10^{-4} \text{ deg} = 0.176 \text{ arc second}\end{aligned}$$

$$\begin{aligned}\Theta_{S_{rms}} &= \frac{1}{3.6} \sqrt{\frac{\pi}{2 \times 1} (9.0 + 1) (2 \times 10^{-11})} \\ &= 0.493 \times 10^{-5} \text{ deg} = 0.018 \text{ arc second}\end{aligned}$$

The total rms pointing uncertainty is given by:

$$\begin{aligned}\Theta_{rms} &= \sqrt{\Theta_{T_{rms}}^2 + \Theta_{S_{rms}}^2} = \sqrt{(0.176)^2 + (0.018)^2} \\ &= 0.185 \text{ arc second}\end{aligned}$$

Therefore, the control loop should be capable of holding the rms pointing uncertainty to 0.2 arc second.

Specification for Fluidic Proportional Thruster - The Performance and Design Specifications for Fluidic Proportional Thruster (Spec. No. A1539), were defined by coordinated effort between NASA/ARC and the General Electric Company. These Specifications are based on the hybrid computer simulation and noise analysis results. The hybrid computer simulation provides data on the minimum acceptable thrust level to insure a successful SPARCS mission. It also sets the required FPT dynamic performance. The noise analysis fixes a maximum value on the thrust noise power spectral density so that the rms pointing jitter of a SPARCS payload will not exceed 0.2 arc seconds. Also included in the Specification are size and weight requirements to insure the FPT can be mounted inside an existing SPARCS insert. Specification No. A14359 was submitted and approved by NASA/ARC prior to detailed hardware design.

#### HARDWARE IMPLEMENTATION

##### Summary

The Inspection Plan for Fluidic Proportional Thruster was submitted and approved early in the program. Concurrently the torque motors, vortex valves, solenoid valves and orifices were designed using conventional design techniques.

##### Discussion

Inspection Plan for Fluidic Proportional Thruster - The Inspection Plan (SFO No. 1) submitted during the program is a document prepared by GE and approved

by NASA/ARC. It provides for controlling the quality of manufacturing and assembly of the FPT and defines the inspection system to be used on Contract NAS 2-5466. The Inspection Plan provides the authority for the inspection system management. Specifically, the inspection system is controlled by:

1. Drawings
2. Specifications
3. Summary work instructions
4. Work instructions
5. Special instructions
6. Engineering change orders (E.C.O.'s)

The Inspection Plan was complied with by the GE Specialty Fluidics Shop Operation throughout the program.

Thrust Nozzles - The thrust nozzle size is fixed by the maximum pressure the FPT can produce in a thrust nozzle chamber and on the required thrust. The maximum nozzle pressure is limited by the FPT's three commercially available dry coil torque motors which should not be exposed to pressures exceeding 2000 psi; and because the vendor, D. G. O'Brien, Inc., expressed reservation about operation at 2000 psi, it was decided to restrict the pressure at the torque motor from exceeding 1000 psi. This restriction in turn limits the nozzle chamber pressure to values not exceeding about 350 psi. With this nozzle chamber pressure limitation it was decided to specify thrust nozzles with 0.067 inch throat diameters because that satisfies system thrust requirements. In addition to the nozzle throat diameter a bell-shaped nozzle with a 15:1 expansion ratio was suggested. The effective thrust coefficient is 1.77. Although the nozzles are not deliverable items, their size was specified to complete the design.

Vortex Valve Specification - The vortex valve outlets ( $D_o$ ) are determined from the thrust nozzle throat diameter ( $D_t$ ) by the following relationships:

$$D_o = \sqrt{\frac{1}{2 C_D} \left( \frac{P_o}{P_v} \right)} D_t \quad \text{in the pitch and yaw channels}$$
$$D_o = \sqrt{\frac{1}{C_D} \left( \frac{P_o}{P_v} \right)} D_t \quad \text{in the roll channel}$$

where:  $P_o/P_v = 0.6$  pressure ratio across the vortex valve  
 $C_D = 0.65$  discharge coefficient  
 $D_t = 0.067$  inches thrust nozzle throat diameter

If these values are substituted in the expressions for  $D_o$ , the results are:

Vortex valve outlet diameter  $D_o = 0.045$  in. (pitch and yaw)  
 $D_o = 0.065$  in. (roll)

The control port areas are roughly proportional to the outlet areas. The results are:

Control area  $A_c = 2.5 \times 10^{-4}$  in<sup>2</sup> (pitch and yaw)  
 $A_c = 5.5 \times 10^{-4}$  in<sup>2</sup> (roll)

For this program the spin chamber diameter was fixed once the manifold design was set. The result which is compatible with the vortex valve outlet area is:

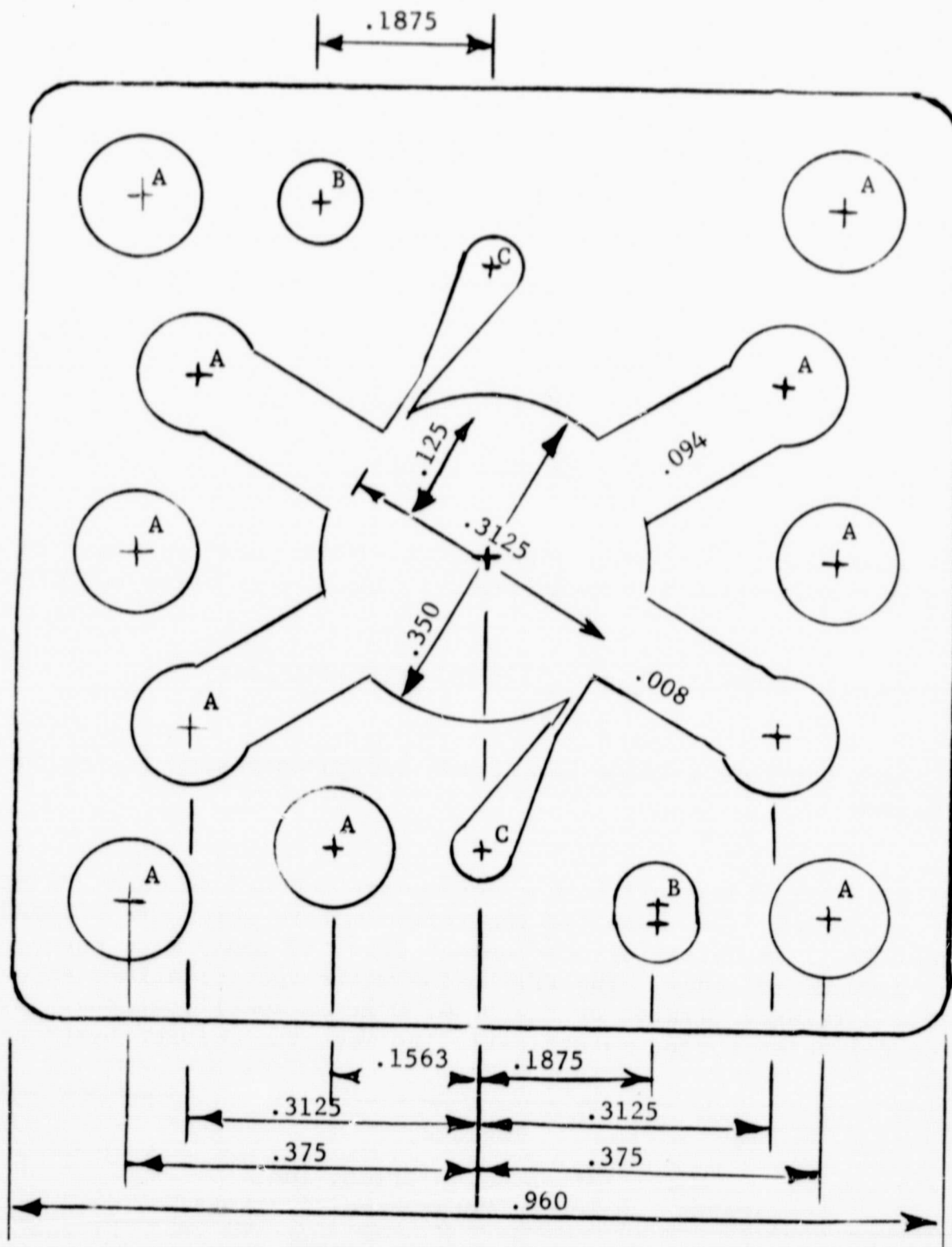
Spin chamber diameter  $D_s = 0.3125$  in. (all channels)

Figure 14 shows the vortex valve lamination design corresponding to the specified dimensions.

Torque Motors - Three dry coil torque motors are mounted on each FPT manifold body. D. G. O'Brien, Inc. supplied the torque motors which are a standard model (Model 121). Substantial development time and money were saved by purchasing a standard model. The FPT torque motor specifications shown in Table 2 are a relaxed version of the D. G. O'Brien specifications. Even so, some of the delivered torque motors failed to meet the relaxed hysteresis specification.

Stroke	$\pm 0.006$ in.
Mid-position force at rated current	1.2 lb
End-of-stroke force at rated current	.65 lb
Stroking position below base	0.35 in.
Hysteresis, % of rated current, max	2%
Resonant frequency, unloaded	500 Hz
Rated input power	2 watts
Proof pressure	5000 psi
Max operating temperature	275F
Net spring constant at stroking position	80 to 120 lb/in with 100 lb/in nominal
Weight	3.5 oz
Resistance per coil	250 ohms
Electrical self time constant L/R	.001 sec





Holes: A = .125 Dia.  
 B = .094 Dia.  
 C = .070 Dia.

Figure 14  
 SPARCS FPT Vortex Valve Lamination

An analysis of the torque motor performance indicates the Model 121 will exceed the SPARCS 150 mission requirements and can meet the SPARCS 350 minimum mission requirements. The analysis included the following:

1. Stability of the inverted flapper configuration with the Model 121 torque motor.
2. Capability of the Model 121 torque motor for 100% rated flapper displacement in the absence of positive pressure feedback.
3. Capability of the Model 121 torque motor to pull the flapper out of the hardover position with maximum positive pressure feedback.

Solenoid Valves - The FPT requires four solenoid valves. One valve opens the main supply line out of the Freon 14 supply tank at the mission commencement and remains activated for the duration of the mission. The other three solenoid valves control the flow levels (coarse or fine) through each of the three FPT thrust channels. These solenoids are activated in an unpredictable fashion throughout a SPARCS mission.

NASA/ARC recommended using Sterer solenoid valves which were previously developed on the SPARCS program. NASA supplied nine solenoids as GFE on Contract NAS 2-5466. The GFE solenoids designed for operation with 5000 psi across them were retro-fitted with back-up plates to enable operation at high pressures. At NASA/ARC's recommendation acceptance tests were limited to an initial tank pressure of 4500 psig. One of the solenoids malfunctioned at pressures above 3000 psig.

## HARDWARE FABRICATION

### Summary

The FPT consists of three torque motors, four solenoid valves, six vortex valves and a manifold to which all the components are mounted. The successful fabrication of the manifold by a numerical control (NC) machine represents a major manufacturing achievement under this contract because it demonstrated the feasibility of repeatable semi-automatic fabrication of future FPT manifolds.

### Discussion

A functional schematic diagram of the FPT was shown previously in Figure 2. It includes a supply shutoff solenoid valve, three thrust level select solenoid valves, three torque motors, three pairs of vortex valves, and fill line check valves. The FPT is activated by energizing the supply shutoff valve (SV-1). Each channel is supplied through a thrust level select solenoid valve in parallel to a fixed orifice. For high thrust level operation, the solenoid valve is energized so

that the channel is supplied through both paths. Conversely, de-energizing the solenoid valve supplies flow through a smaller area and decreases the channel thrust level. The electrical command to each channel is introduced into the FPT at the electromagnetic torque motors which drive flapper-nozzle valves. The output of the flapper-nozzle is a differential pressure controlling a pair of vortex valves in push-pull. The outputs of the vortex valve go to the thrust nozzles.

Figure 15 is the FPT outline drawing. The main body of the FPT package is the manifold, and its design and manufacture constituted a major accomplishment under this contract. The manifold is compact and, because it is formed by a numerically controlled (NC) machine, it is relatively easy to produce. With this manifold the FPT total space envelope is approximately 4 x 5 x 7½ inches and the package weighs slightly less than seven pounds.

The NC machine is controlled by a work plan whose instructions are recorded on punched tape. The generation of the punched tape represents a major portion of the effort in running the NC machine. The NC machining program (as recorded on punched tape) and the manufacturing fixtures first were checked out by rough machining a full scale plexiglas model (Figure 16). The complexity of the passage drilling in the FPT housing warranted this three dimensional layout design check. The final manifolds were fabricated from 7075 aluminum by the NC machine.

## HARDWARE EVALUATION

### Summary

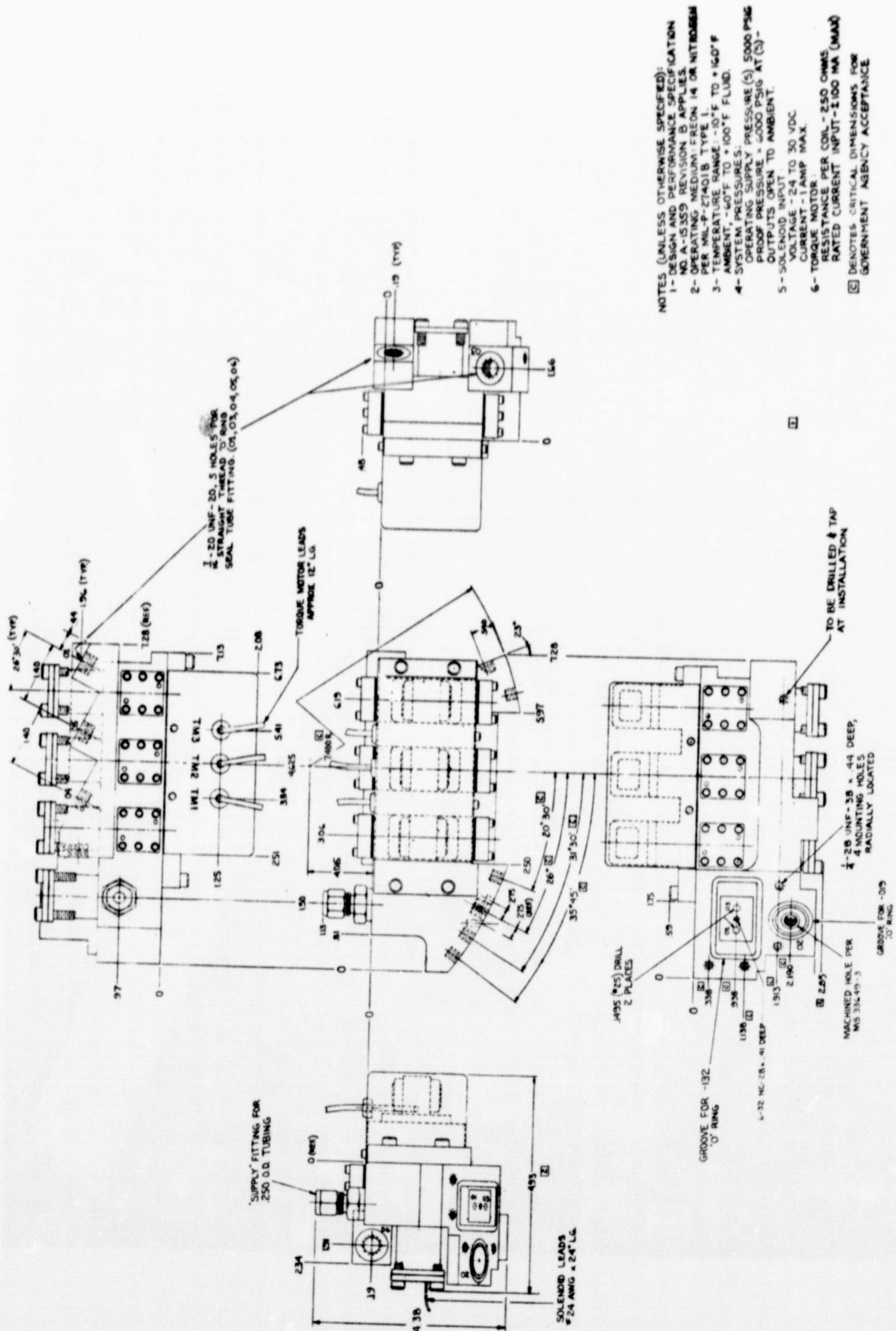
The Acceptance Test Procedure (ATP) was written by General Electric Co. and approved by NASA/ARC. An elaborate laboratory facility for performing the tests called for in the ATP was assembled. Typical mission commands were preprogrammed into an automated sequence controller and the salient sequential output data were traced on an multi-channel recorder and on x-y plotters. Two FPT's successfully passed the ATP requirements and were shipped to NASA/ARC.

### Discussion

Acceptance Test Procedure - The ATP (SFO No. 2) is a document written by GE and approved by NASA/ARC. The ATP purpose is to translate the performance requirements in the Specification (Spec. No. A-15359) to a set of laboratory tests, the results of which establishes simplified criteria for quality assurance inspection.

ATP Tests - Two FPT's were subjected to the tests called for in the ATP. The ATP calls for four test phases, the first two of which must be completed in 36 seconds as shown in Table 3. Because four performance features must be





NOTES (UNLESS OTHERWISE SPECIFIED):

- 1- DESIGN AND PERFORMANCE SPECIFICATION NO. A-5355 REVISION B APPLIES.
- 2- OPERATING MEDIUM: FREON 14 OR NITROGEN PER MIL-P-27401B TYPE 1.
- 3- TEMPERATURE RANGE: -10°F TO +160°F AMBENT, -60°F TO +100°F FLUID.
- 4- SYSTEM PRESSURES: OPERATING SUPPLY PRESSURE (S), 5000 PSIG PROOF PRESSURE = 6000 PSIG AT (S) - OUTPUTS OPEN TO AMBIENT.
- 5- SOLENOID INPUT: VOLTAGE - 24 TO 30 VDC CURRENT - 1 AMP MAX.
- 6- TORQUE MOTOR: RESISTANCE PER COIL - 250 OHMS RATED CURRENT INPUT - 1.100 MA (MAX)

☐ DENOTES CRITICAL DIMENSIONS FOR GOVERNMENT AGENCY ACCEPTANCE

Figure 15

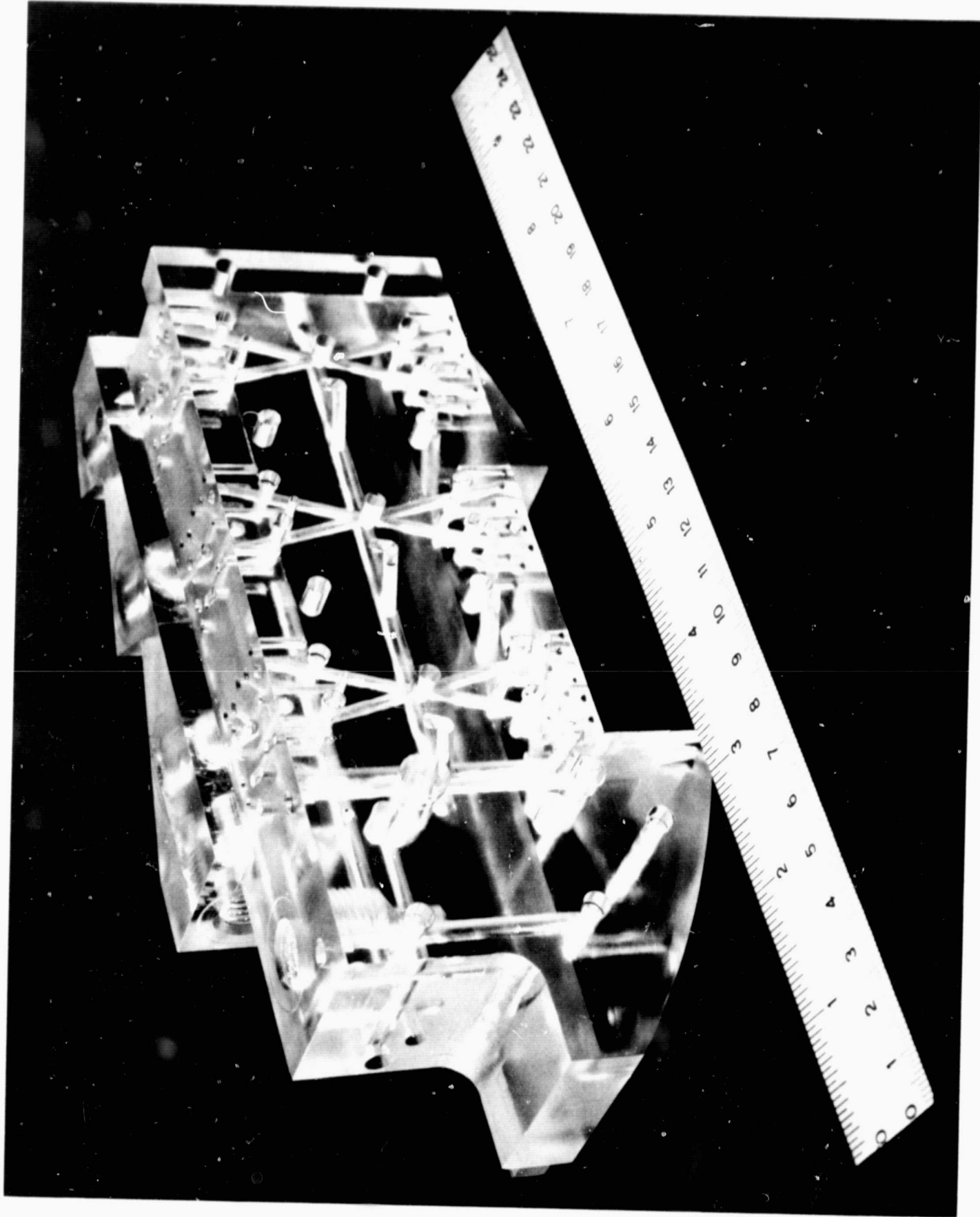


Figure 16 - Plexiglas Model of FPT Manifold

Table 3  
FPT Functional Test Outline

Test Mode	Phase I		Phase II			Phase III			Phase IV	Pressure Check
	Coarse Acquisition	Fine Acquisition	Proportional Action	Null Offset	Hysteresis Static Gain Offset	Dynamic Test	Noise	Null Offset		
Test Paragraph	3.2.3.2	3.2.3.3.2	.3	.4	3.2.4.2.2	.3	.4	3.2.4.3	3.2.4.4	
Test Parameter	$\Delta P$ per Fig. 3.2.3 3.2.4	$\Delta P$ per Fig. 3.2.3 3.2.4	$\Delta P$ Decreases	$\Delta P$ per Figure 3.2.5	$\Delta P$ vs Input	$\Delta P$ vs Input	$\Delta P$ Noise	$\Delta P$ vs Input	Tank Pressure & Temperature	
Elapsed Time (sec)	0-16	16-18	18-26	26-36	No	Requirement	Requirement	1.5		
Total Time (sec)	16	20	20	20	No	Requirement	Requirement	Hour		
SV 1	Open	Open	Open	Open	Open	As Required	As Required	Open	Closed	
SV 2	28 volt	Closed			Closed			Closed	Closed	
SV 3										
SV 4										
TM 1	3.8 volt	3.8 V	Decrease to zero in 8 sec	No Input	2 V	.2 V	No Input	No Input	No Input	
TM 2										
TM 3	2 Hz	2 Hz			Vary slowly	2 Hz				
Tank Pressure	5000-1600	1600-1400			1000 Regulated	1000 Regulated		700 Regulated	2000	
Gas	CF <sub>4</sub>	CF <sub>4</sub>			CF <sub>4</sub>	CF <sub>4</sub>		CF <sub>4</sub>	N <sub>2</sub>	
Instrumentation	3.2.3.2.1	3.2.3.2.1			3.2.3.-2.1			3.2.3.2.1	3.2.4	



sequentially tested in the first two phases, it facilitates repeatability to automate this portion of the ATP. This was done by slaving the sequential events to wiper positions on a rotary stepper switch (similar to those in older telephone exchanges) and pulsing the switch at a 0.5 Hz rate. The stepper switch with some auxiliary electronic circuits comprised the command generator (Figure 17). The periphery equipment around the command generator provides inputs to it. The command generator uses these inputs to advance the stepper switch and drive the electronic circuits. The command generator outputs are four solenoid actuation signals and three torque motor command signals. All of these signals are accurately sequenced because they are slaved to the stepper switch position in the command generator.

The command generator outputs go to the FPT inputs as shown in Figure 18. Also shown on that figure are sensed and recorded outputs. For ATP Phases I and II the FPT inputs come in automatically and are recorded along with the FPT outputs. In Phases I and II verification of coarse and fine acquisition operation, proportional action in the fine thrust mode and a reasonably small null offset is established.

For Phases III and IV the command generator is removed from the FPT inputs, and inputs are manually provided. This is acceptable because the tests in the latter two phases do not rely on accurate sequencing of signals.

In Phase III hysteresis, static gain, null offset, dynamic response and noise power spectral density are measured. These performance indicators determine the ability of the FPT to meet the pointing stability goal of 0.2 arc second rms. Phase IV is devoted to measuring the null offsets. The null offsets determine how accurately the vehicle can point on an absolute basis. For example, the null offset requirement in Phase IV is selected so that the absolute pointing accuracy in pitch and yaw will fix the vehicle within a 14.5 arc second cone half angle from the absolutely perfect pointing direction. The Phase III requirements are selected so that the jitter in the pointing will have an rms value not exceeding 0.2 arc seconds.

Figures 19 and 20 are photographs of some of the ATP laboratory facilities. The top of Figure 19 shows the test set-up including the strip recorders (on right), power supplies and signal generators (lower center), command generator (center) and the Freon supply (center left). The bottom of Figure 19 shows the explosion shield with the PAGE control cable (top), supply bottle (right) and the steam ejector pipe over the supply bottle. The top of Figure 20 shows the system connection for charging with the blow-down tank in the explosion shield in the lower left, the thermocouple ice junction next to the explosion shield and the PAGE high pressure outlet in the center. The bottom photograph in Figure 20 shows the command signal generator.

The results of the acceptance tests conducted on the two FPT's delivered on the contract are summarized in the Acceptance Test Report forms shown on pages 32 to 35.

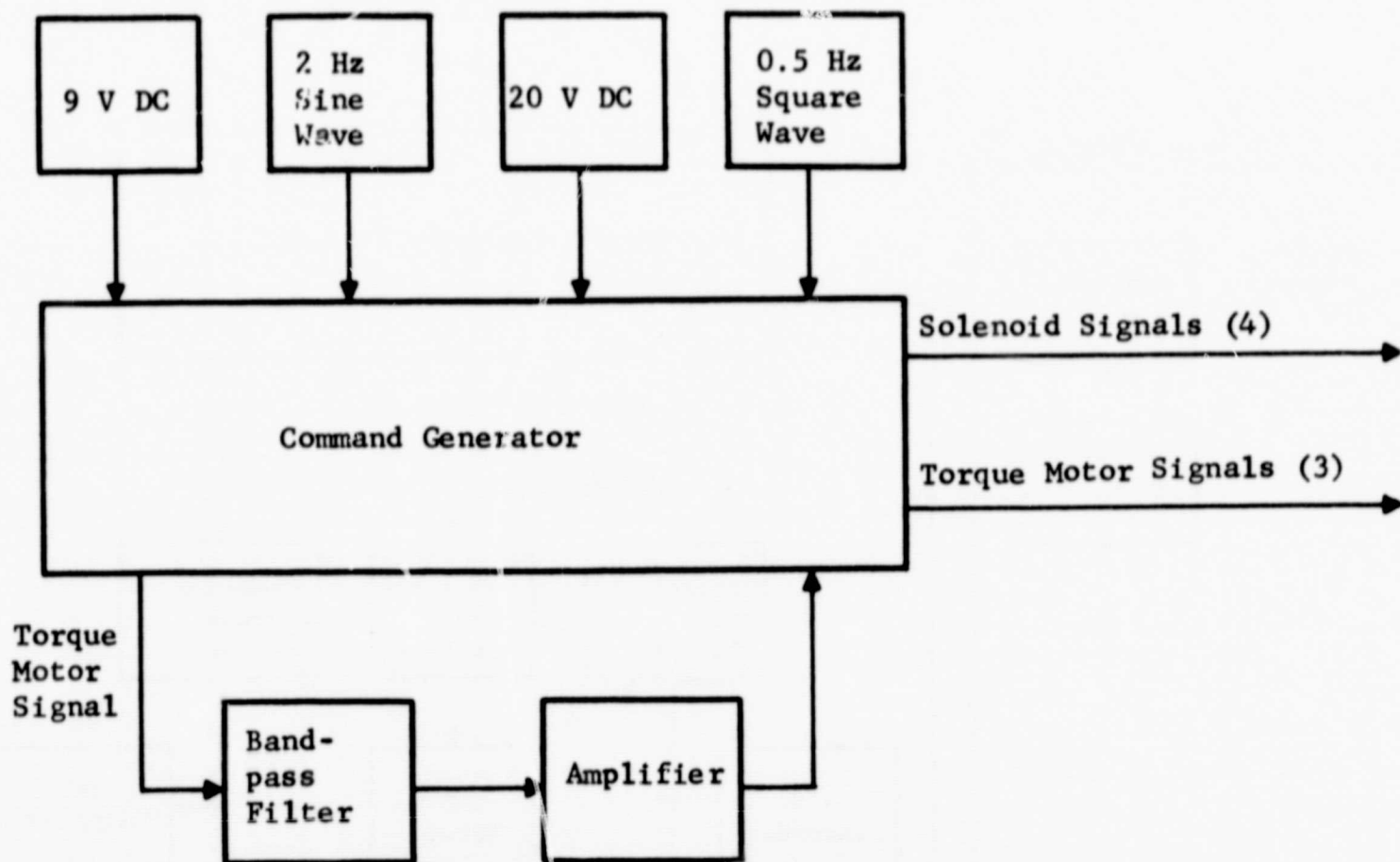


Figure 17  
 Functional Schematic of Laboratory Facility  
 for Automating Phases I and II of ATP

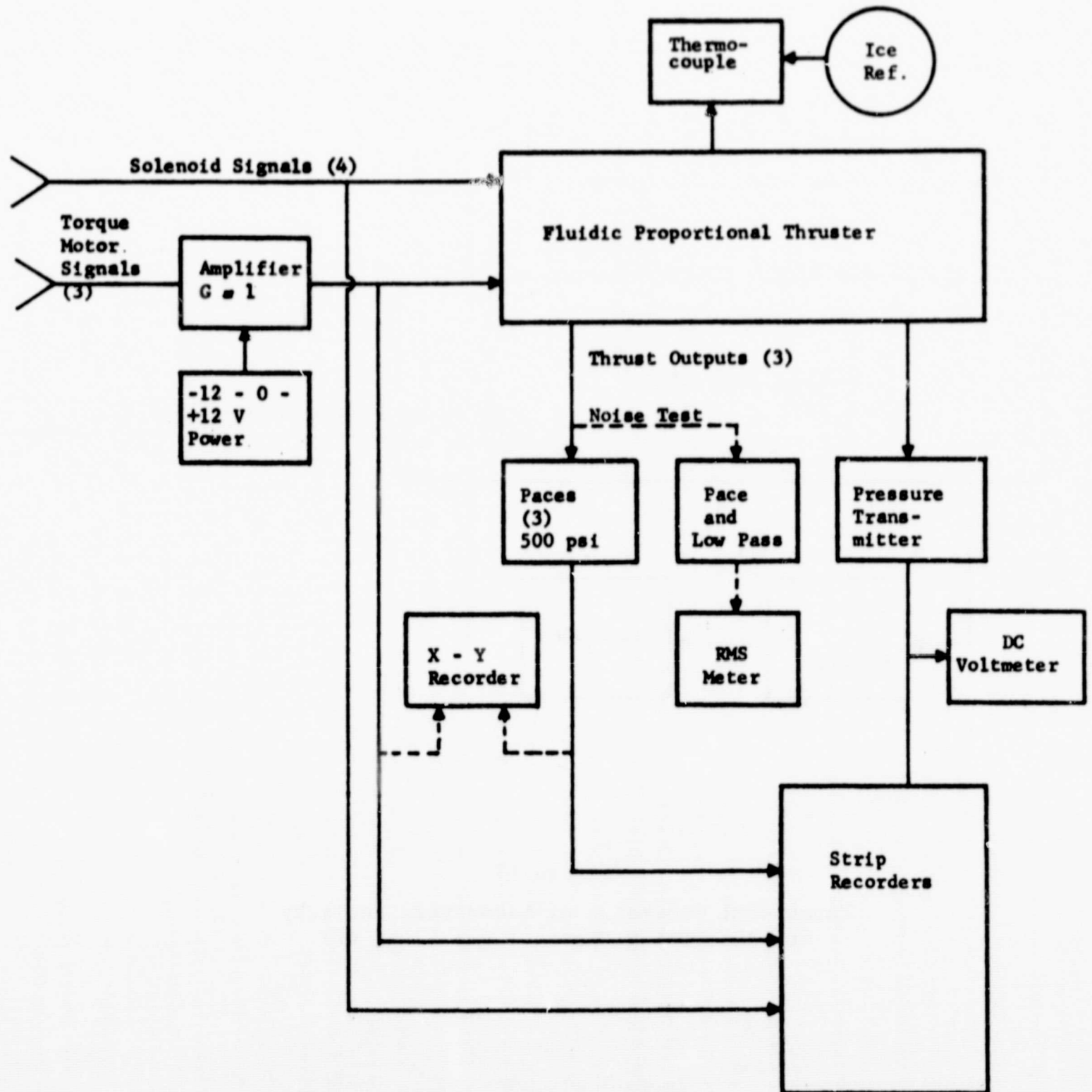
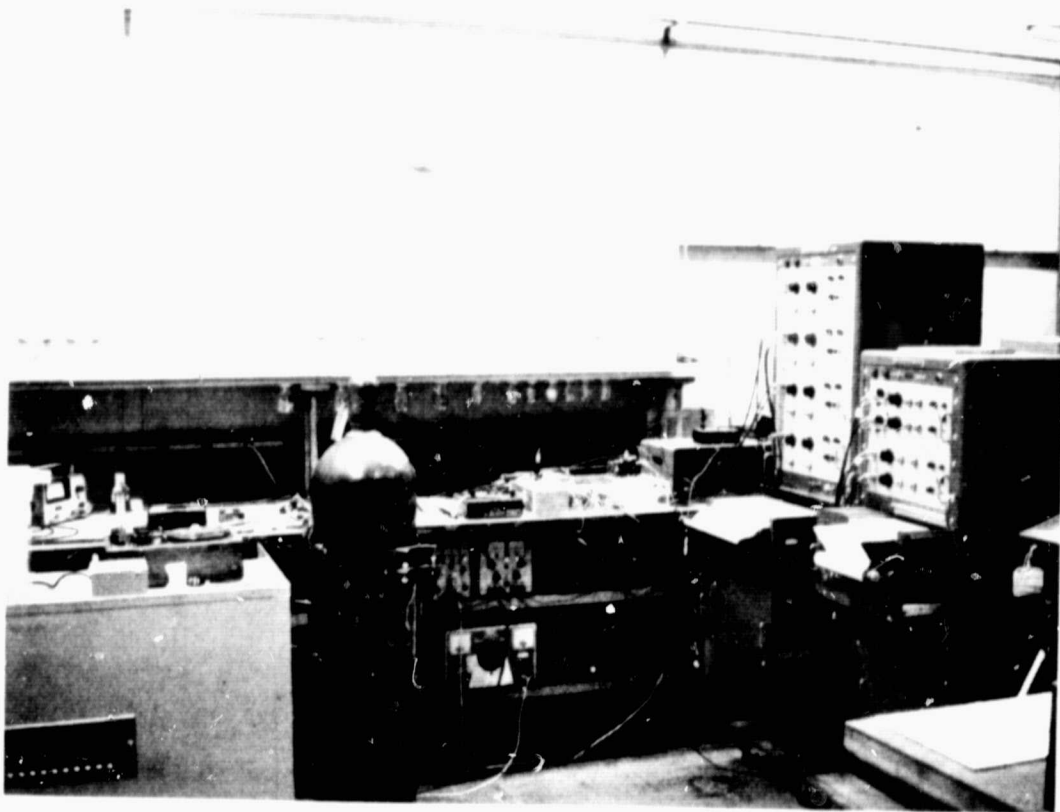
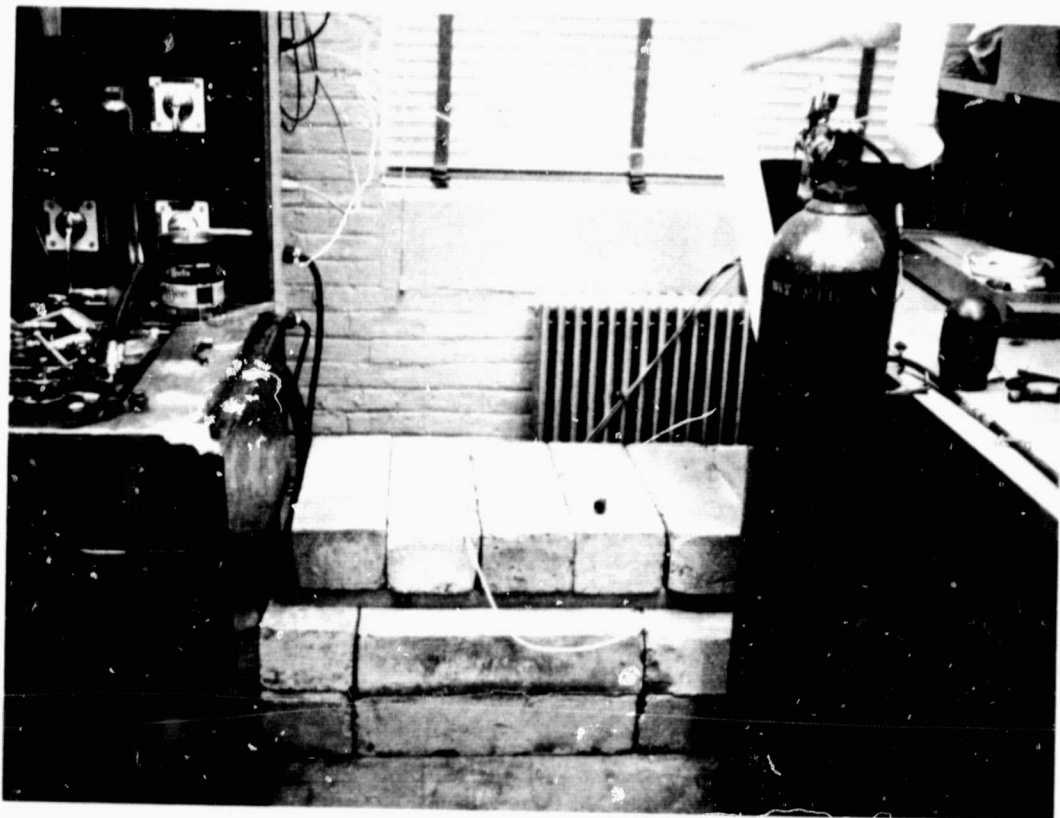


Figure 18 - Functional Schematic of the FPT, Input Driving Signals and Output Transducers



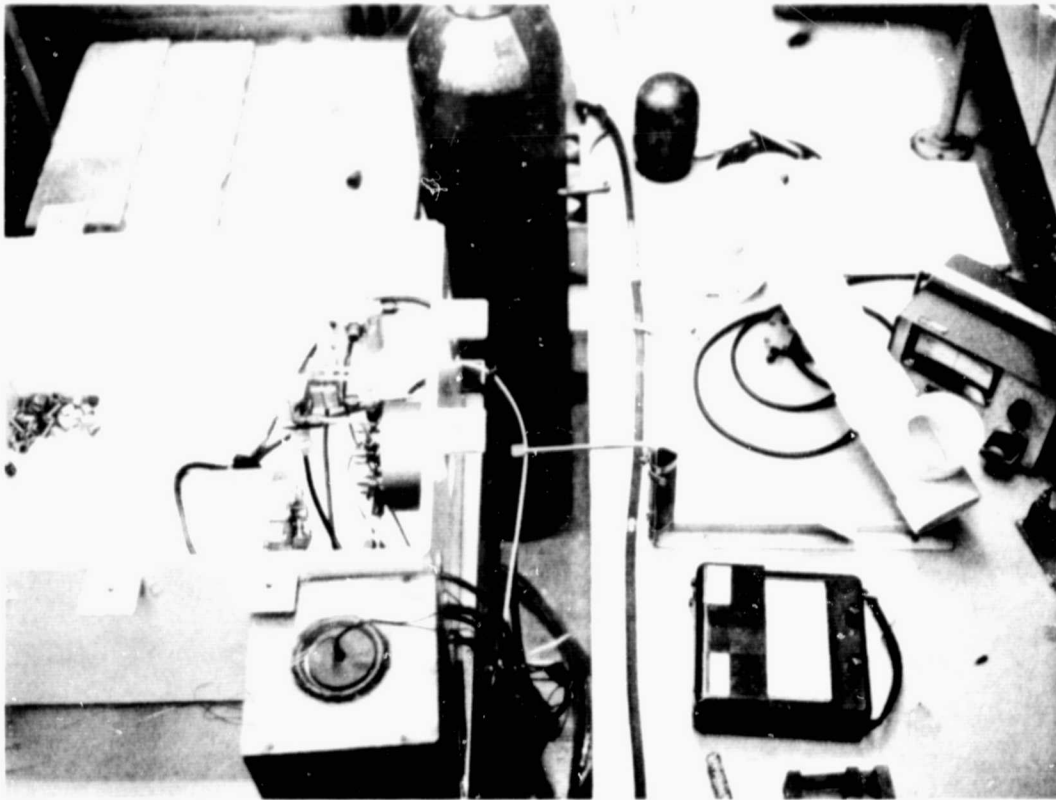


ATP Test Set-up

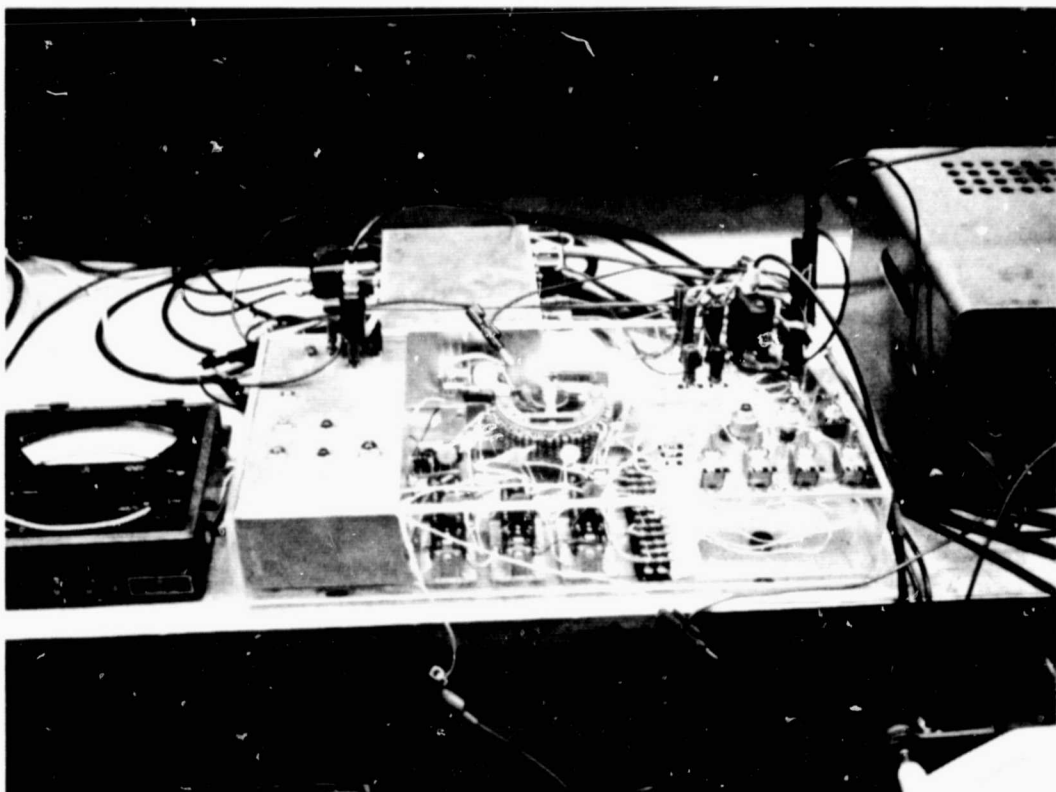


Explosion Shield Containing PAGE

Figure 19



System Connection for Charging



Command Signal Generator

Figure 20

# GENERAL ELECTRIC COMPANY

1 RIVER ROAD, SCHENECTADY, NEW YORK 12305 . . . TELEPHONE (518) 374-2211

**SPECIALTY FLUIDICS  
OPERATION**

NEW BUSINESSES  
DEVELOPMENT OPERATION

Prepared by: T.S. Honda 11/5/70 <i>JSH</i>	<b>ACCEPTANCE TEST REPORT</b>	Date: 11/5/70
Approved by: <i>JNS</i>	Component: SPARCS IV Fluidic Proportional Thruster	Serial No. 24PT11AA0001

Prepared for: NASA/Ames Research Center      Spec. No. A-15359 Rev. A

Contract No.: NAS 2-5466

Tested per Acceptance Test Procedure SFO-2, Rev. A

ATP Par. No.	Parameter Description	Specification			Actual Reading
		Min	Max	Units	
3.1	Examination of Product - component meets requirements of workmanship identification, marking, finish and conforms to GE Drawings 423D176 Rev 1 and 587E704 Rev 3.				Yes
3.2.2.1	Torque Motor Resistances				
	Pitch SN A7948	--	125	ohms	123
	Yaw SN A7940	--	125	ohms	122
	Roll SN A7947	--	125	ohms	123
3.2.3.2	Phase I Coarse Acquisition	Strip Record			Function OK
3.2.3.2.2	Coarse Saturation Limits				
	Pitch/Yaw $\Delta P$ Fig. 3.2.3	.067 P <sub>s</sub>	--	psid	.100 P <sub>s</sub>
	Roll $\Delta P$ Fig. 3.2.4	.067 P <sub>s</sub>	--	psid	.094 P <sub>s</sub>
3.2.3.3	Phase II Fine Acquisition	Strip Record			Function OK
3.2.3.3.2	Fine Saturation Limits				
	Pitch/Yaw $\Delta P$ Fig. 3.2.3	.0135 P <sub>s</sub>	--	psid	.025 P <sub>s</sub>
	Roll $\Delta P$ Fig. 3.2.4	.00335 P <sub>s</sub>	--	psid	.006 P <sub>s</sub>
3.2.3.3.3	Proportional Action	Strip Record			Function OK
3.2.3.3.4	Null Offset Fig. 3.2.5				
	Pitch/Yaw	--	.0027 P <sub>s</sub>	psid	.0014 P <sub>s</sub> / .0007 P <sub>s</sub>
	Roll	--	.00068 P <sub>s</sub>	psid	.00039 P <sub>s</sub>



GENERAL  ELECTRIC

ATP Par. No.	Parameter Description	Specification			Actual Reading
		Min	Max	Units	
3.2.4.2.2	Phase III				
3.2.4.2.2.1	Hysteresis (Pitch/Yaw/Roll)	--	3	%	2.2/2.0/1.8
3.2.4.2.2.2	Static Gain Pitch/Yaw	.03 P <sub>s</sub>	.06 P <sub>s</sub>	psid/volt	.045 P <sub>s</sub>
	Roll	.006 P <sub>s</sub>	.012 P <sub>s</sub>	psid/volt	.01 P <sub>s</sub>
3.2.4.2.2.3	Null Offset Pitch/Yaw	--	.0027 P <sub>s</sub>	psid	.0013 P <sub>s</sub>
	Roll	--	.00068 P <sub>s</sub>	psid	.00039 P <sub>s</sub>
3.2.4.2.3	Dynamic Test Phase Lag	--	26	degrees	26.7
3.2.4.2.4	Noise	--	$7 \times 10^{-10} P_s^2$	psid <sup>2</sup> /Hz	$6.1 \times 10^{-10} P_s^2$ to $7.9 \times 10^{-10} P_s^2$
3.2.4.3	Phase IV Null Offset: Pitch/Yaw	--	.0027 P <sub>s</sub>	psid	.00073 P <sub>s</sub>
	Roll	--	.00067 P <sub>s</sub>	psid	.00055 P <sub>s</sub>
3.2.4.4	Tank Pressure Hold	$P_2 = .9 P_1 \left[ \frac{T_2}{T_1} \right]$	--	psia	$P_2 = P_1 \left[ \frac{T_2}{T_1} \right]$

# GENERAL ELECTRIC COMPANY

1 RIVER ROAD, SCHENECTADY, NEW YORK 12305 . . . TELEPHONE (518) 374-2211

**SPECIALTY FLUIDICS  
OPERATION**

NEW BUSINESSES  
DEVELOPMENT OPERATION

Prepared by: T. S. Honda <i>TH</i>	ACCEPTANCE TEST REPORT	Date: December 16, 1970
Approved by: <i>J. J. Stephens</i>	Component: SPARCS IV Fluidic Proportional Thruster	Serial No. 24PT11AA0002

Prepared for: NASA/Ames Research Center Spec. No. A-15359 Rev. A

Contract No.: NAS 2-5466

Tested per Acceptance Test Procedure SFO-2, Rev. A

ATP Par. No.	Parameter Description	Specification			Actual Reading
		Min	Max	Units	
3.1	Examination of product: Component meets requirements of workmanship, identification, marking, finish and conforms to G.E. drawings 423D176 Rev. 1 and 587E704 Rev. 3.				yes
3.2.2.1	Torque Motor Resistances				
	Pitch SNA7952	-	125	ohms	125
	Yaw SNA7953	-	125	ohms	125
	Roll SNA7949	-	125	ohms	125
3.2.3.2	Phase I Coarse Acquisition	Strip Record			Function OK
3.2.3.2.2	Coarse Saturation Limits				
	Pitch/Yaw $\Delta P$ Fig. 3.2.3	.067 P <sub>s</sub>	-	psid	.11 P <sub>s</sub>
	Roll $\Delta P$ Fig. 3.2.4	.067 P <sub>s</sub>	-	psid	.10 P <sub>s</sub>
3.2.3.3.3	Proportional Action	Strip Record			Function OK
3.2.3.3.4	Null Offset Fig. 3.2.5				
	Pitch/Yaw	-	.0027 P <sub>s</sub>	psid	.0026 P <sub>s</sub> / .0007 P <sub>s</sub>
	Roll	-	.00068 P <sub>s</sub>	psid	.0007 P <sub>s</sub>
3.2.4.2.2	Phase III				
3.2.4.2.2.1	Hysteresis (Pitch/Yaw/Roll)	-	3	%	2.4/2.5/2.5

GENERAL  ELECTRIC

ATP Par. No.	Parameter Description	Specification		Units	Actual Reading
		Min	Max		
3.2.4.2.2.2	Static Gain Pitch/Yaw Roll	.03 P <sub>S</sub> .006 P <sub>S</sub>	.06 P <sub>S</sub> .012 P <sub>S</sub>	psid/volt psid/volt	.045P <sub>S</sub> /.04P <sub>S</sub> .0088 P <sub>S</sub>
3.2.4.2.2.3	Null Offset Pitch/Yaw Roll	- -	.0027 P <sub>S</sub> .00068P <sub>S</sub>	psid psid	.0023P <sub>S</sub> /.0005P <sub>S</sub> .0006 P <sub>S</sub>
3.2.4.2.3	Dynamic Test Phase Lag	-	30	degrees	26
3.2.4.2.4	Noise		$5.5 \times 10^{-80} P_s^2$	psid <sup>2</sup> /Hz	$9.15 \times 10^{-10} P_s^2$ to $2 \times 10^9 P_s$
3.2.4.3	Phase IV Null Offset Pitch/Yaw Roll	- -	.0027 P <sub>S</sub> .00067P <sub>S</sub>	psid psid	.002P <sub>S</sub> /.0002P <sub>S</sub> .00043 P <sub>S</sub>
3.2.4.4	Tank Pressure Hold		$P_2 = .9P_1 \left[ \frac{T_2}{T_1} \right]$	psia	$P_2 = P_1 \left[ \frac{T_2}{T_1} \right]$